Early Noise Exposure and Changes in Medial Olivocochlear Strength Alters Auditory Pathway Development

Authors: Valeria C. Castagna[1,2], Luis E. Boero[1,2], Mariano N. Di Guilmi[1], Paul A. Fuchs[3], Amanda M. Lauer[3], Ana Belén Elgoyhen[1,2] and Maria Eugenia Gomez-Casati[2]

Affiliations: [1]Instituto de Investigaciones en Ingeniería Genética y Biología Molecular, Dr. Héctor N. Torres, Consejo Nacional de Investigaciones Científicas y Técnicas, 1428 Buenos Aires, Argentina.

[2]Instituto de Farmacología, Facultad de Medicina, Universidad de Buenos Aires, 1121 Buenos Aires, Argentina and Consejo Nacional de Investigaciones Científicas y Técnicas, Argentina.

[3]Departments of Otolaryngology-HNS, Neuroscience, and Functional Anatomy and Evolution, Johns Hopkins University, School of Medicine, Baltimore, Maryland 21205, United States.

Corresponding Author: María Eugenia Gómez-Casati, Ph.D.
Instituto de Farmacología. Facultad de Medicina. Universidad de Buenos Aires.
Address: Paraguay 2155. C1121ABG, Buenos Aires, Argentina.
Phone: 54-11-52853350
E-mail: mgomezcasati@fmed.uba.ar, megomezcasati@gmail.com

Conflict of Interest: The authors declare no competing financial or non-financial interest.

Acknowledgements: This research was supported by Agencia Nacional de Promoción Científica y Técnica (Argentina) to M.E.G-C and NIH Grant R01 DC001508 (A.M.L and A.B.E).

Author Contributions: V.C.C, L.E.B, M.N.D-G, P.A.F, A.M.L, A.B.E and M.E.G-C designed research; V.C.C performed experiments; V.C.C analyzed data. M.E.G-C wrote the paper. All authors discussed the results, read, edited, and commented on the manuscript.

ABSTRACT

Periodic spontaneous activity is a key feature of developing sensory systems, essential for the formation and refinement of neural circuits. Before the onset of hearing in altricial mammals, cochlear inner hair cells exhibit spontaneous electrical activity that activates primary afferents to propagate into the central nervous system. This activity, modulated by the medial olivocochlear efferent feedback via α9α10 nicotinic cholinergic receptors present in inner hair cells, is crucial for auditory system maturation. In this study, we examined the impact of sound exposure at levels below those causing hair cell damage during the critical developmental period by using genetically modified mice - α9 knockout and α9 knock-in models - with either absent or enhanced cholinergic activity. We further assessed how varying levels of medial olivocochlear feedback interact with early-age noise exposure to affect auditory development. Our findings reveal that both increased and absent olivocochlear activity result in altered auditory sensitivity at the onset of hearing and affect ribbon synapse number and morphology. Additionally, early exposure to loud noise caused long lasting changes in the inner ear of wild-type and α9 knockout mice, underscoring the heightened vulnerability during early development. In contrast, mice with enhanced cholinergic activity were protected from these changes. Overall, this work highlights the critical role of medial olivocochlear modulation in proper auditory system development and indicates that early noise exposure can interfere with normal cochlear maturation, resulting in pronounced long-term effects.

INTRODUCTION

Cochlear inner hair cells (IHCs) and afferent neurons in altricial mammals exhibit spontaneous electrical activity that propagates into the central nervous system (CNS) prior to the onset of hearing, which occurs around postnatal day 12 (P12) (1–5). This spontaneous firing is thought to be crucial for promoting neuronal survival in early auditory centers, driving their maturation, and shaping their synaptic connections through activity-dependent mechanisms (6–11). In the mouse cochlea, spontaneous activity in IHCs arises at late embryonic stages, triggered by ATP release from adjacent inner supporting cells and relies on interactions between depolarizing Ca^{2+} currents and repolarizing K^{+} currents (2, 4, 12–14).

Before the onset of hearing, IHCs' spontaneous activity is modulated by transient efferent feedback from medial olivocochlear (MOC) neurons descending from the superior olivary complex in the brainstem. These MOC endings form axosomatic synaptic contacts with immature IHCs via α9α10 nicotinic cholinergic receptors (nAChRs), coupled to Ca^{2+}-dependent SK2 channels, resulting in hyperpolarization of IHCs (15–17). This transient efferent innervation is thought to shape burst firing patterns, guiding the normal functional development of IHCs' synaptic machinery and ensuring the establishment of bilateral neural representation in the developing CNS (10, 11, 18, 19). As IHCs mature, they lose direct efferent contacts and no longer respond to acetylcholine (ACh). Thus, in adult mice MOC fibers synapse exclusively with OHCs (20, 21). The MOC reflex in adulthood is thought to regulate hearing's dynamic range (22), enhances signal detection in noisy environments (23–25), contributes to selective attention (26), provides protection from noise-induced hearing damage (27–31) and helps slow cochlear aging (32, 33).

During the postnatal period around the onset of hearing, the cochlea and central auditory system undergo significant structural and functional changes with ongoing refinement continuing at different levels of the auditory pathway. While maturation at the auditory cortex level is typically reached around P40, certain structures, such as the endbulbs of Held in the brainstem, continue

to refine their synaptic architecture beyond this time frame, up to approximately postnatal week 9 (34–38). Several studies have shown that sound exposure during development significantly contributes to the functional shaping of the structural organization and signal processing capabilities of the mammalian auditory system (34, 39–41). Early acoustic exposure influences neuronal sensitivity, innervation, frequency tuning and response characteristics of neurons at multiple levels of the auditory pathway (35–37, 42–44). Nevertheless, the extent to which ascending and descending pathways interact with the acoustic environment to shape activity patterns and instruct neuronal circuit formation remain largely unknown. In this study, we queried the effect of the strength of the cholinergic component of the MOC system on auditory system development. We used genetically modified mice with varying levels of α9α10 nAChR activity: α9 knock-out mice (Chrna9 KO; α9KO), which lacks cholinergic transmission between efferent neurons and hair cells (45), and α9 knock-in mice (Chrna9L9'T; α9KI) carrying an α9 point mutation that leads to enhanced MOC activity (29). In addition, we explored the effect of exposure to sound levels below those causing hair cell damage or permanent threshold shifts during this critical period of auditory system development. We demonstrate that alterations in MOC modulation results in changes in auditory sensitivity at the onset of hearing and affect the number and morphology of ribbon synapses of mature IHCs. Moreover, early-age exposure to loud noise produced permanent alterations in auditory sensitivity in wild type (WT) and α9KO mice, indicating the importance of normal patterns of sound-driven activity during the initial stages of auditory development. Notably, the enhancement of cholinergic activity effectively prevented elevations in auditory thresholds and cochlear synaptopathy following noise exposure, even during the early stages of hearing development when the auditory system is still maturing and olivocochlear terminals have recently formed synapses with OHCs (20, 21). Thus, our work contributes to the notion that cochlear efferent modulation during critical developmental periods is essential for establishing proper auditory circuitry. Furthermore, we demonstrate that early noise exposure can

interfere with normal cochlear development, leading to more pronounced long-term consequences.

RESULTS

Onset of auditory perception in mice with different degrees of efferent inhibition

We tracked the onset and development of auditory brainstem responses (ABRs) and distortion-product otoacoustic emissions (DPOAE) at different postnatal ages in mice with distinct levels of α9α10 nAChR activity: 1) WT, with normal MOC function; 2) α9KO, which lacks cholinergic transmission between MOC neurons and hair cells (45), and 3) α9KI mice carrying an α9 nAChR subunit point mutation that leads to enhanced responses to ACh (29). Individual ABR waves reflect the activation of auditory periphery and brainstem processing relay stations within the first ~7 ms after sound stimulus onset (waves 1 to 5). Wave 1 represents the synchrony in firing of spiral ganglion neurons and is highly correlated with the number of synapses between IHCs and auditory nerve fibers, while waves 2-5 represent responses from the ascending auditory pathway (46–51). DPOAEs, sounds recorded from the external auditory canal, assess OHC function. In a healthy cochlea, two close pure tones produce distortions due to OHC nonlinearities, which are amplified by OHC electromotility and detected in the external ear canal (52, 53). Measurements were obtained in anesthetized mice between P12 to P75. Figures 1a and b illustrate that ABR onset, defined as the lowest sound level (<80 dB SPL) at which a discernible wave 1 was observed, occurred earlier in α9KI mice with enhanced MOC function compared to WT mice with normal MOC synapses, and was delayed in α9KO mice lacking α9α10 nAChR activity. Representative ABR traces recorded at P14 in response to a 16 kHz stimulus across varying intensities illustrate differences in ABR thresholds among the three mouse groups with distinct levels of α9α10 nAChR activity (Figure 1a). At this developmental stage, α9KI mice exhibited lower ABR thresholds, and more distinct upward peaks at suprathreshold intensities compared to

WT mice. In contrast, α9KO mice showed higher ABR thresholds relative to WT mice (Figure 1a). Figure 1b shows the mean ABR thresholds measured at test frequencies of 11.33, 16, and 22.65 kHz from P12 to P75 across the three groups of mice. Statistical analysis revealed significant differences among the groups (Kruskal-Wallis, degree of freedom [df] = 2, $p = 0.03$ at 11.33 kHz; $p = 0.02$ at 16 kHz and $p = 0.01$ at 22.65 kHz). α9KI mice exhibited measurable ABR responses as early as P13 and achieved mature threshold levels earlier than their WT littermates (Figure 1b). In contrast, ABR onset was significantly delayed in α9KO mice, particularly at 11.33 and 16 kHz (Kruskal-Wallis, df = 2, $p = 0.04$ at 11.33 and 16 kHz; Figure 1b) indicating that cochlear maturation is slower in the absence of pre-hearing efferent modulation. At P13, no ABR responses were observed in WT (0/9) or α9KO (0/7) mice in response to tone pips at 80 dB SPL across 11.33, 16, and 22.65 kHz. In contrast, 6 out of 9 α9KI mice exhibited ABR responses at P13. By P14, ABR responses were present in 77.7% of WT mice at 11.33 and 22.65 kHz and in 100% at 16 kHz. Meanwhile, 85% of α9KO mice showed responses across all frequencies, although with elevated thresholds compared to WT (Figure 1b and Supplementary Figure 1a). All α9KI mice demonstrated robust responses at all tested frequencies at P14. By P15, response rates reached 100% in WT mice and 91% in α9KO mice. DPOAE responses exhibited a similar trend as ABR thresholds only at 11.33 kHz, although the changes were not statistically significant (Kruskal-Walis, df = 2, $p > 0.05$ at all frequencies; Figure 1c). Note that at P22 and P75, mean ABR and DPOAE thresholds in α9KI mice were slightly elevated by 5–10 dB compared to WT and α9KO mice (Figure 1b, c). This elevation reached statistical significance only for ABR thresholds at P22 (Kruskal-Wallis, df = 2, $p = 0.03$ at 11.33 kHz; $p = 0.04$ at 16 kHz and $p = 0.02$ at 22.65 kHz). The elevated thresholds in α9KI mice at these “mature stages” suggest that this may be due to enhanced cholinergic activity on OHCs, indicating cholinergic MOC effects under resting conditions as previously reported (29). Collectively, these findings indicate that auditory sensitivity is altered at hearing onset in mice with either absent or enhanced cholinergic activity.

Suprathreshold response amplitude for ABR waves 1, 2 and 3 in mice with different levels of α9α10 nAChR activity

ABR individual waves indicate the activation of successive auditory processing centers and can serve as a functional hearing assessment to identify retro-cochlear abnormalities contributing to hearing loss (47–49). Tone pip-evoked ABR waveform amplitudes were analyzed at a suprathreshold level of 80 dB SPL for peaks corresponding to the auditory nerve (wave 1), cochlear nucleus (wave 2), and superior olivary complex (SOC) (wave 3) (50, 51) at different test frequencies in mice with varying levels of MOC strength.

During the early postnatal period, ABR amplitudes were smaller, and the number of discernible upward peaks was fewer in WT and α9KO mice compared to α9KI mice (see representative ABR traces from P13 to P15, Supplementary Figure 1a). Up to P15, response peaks at 80 dB SPL were slightly larger and more distinct in α9KI mice, reflecting their enhanced auditory responses during this critical developmental window. Analysis of ABR wave 1 latencies across different postnatal ages revealed no significant differences between genotypes (Supplementary Figure 1b). At P14, wave 1 latencies were consistently longer across all groups. By P15, latencies stabilized to levels characteristic of mature mice, coinciding with the rapid auditory maturation phase. ABR wave 1 amplitudes increased progressively with postnatal age, reaching a plateau at P22 across all genotypes and frequencies (11.33, 16, and 22.65 kHz; Figure 2a). In WT mice, this increase exhibited a steadier progression compared to that observed in mice with either null or enhanced α9α10 nAChR activity. Notably, ABR wave 1 amplitudes in α9KI mice tended to be slightly larger than those in WT mice up to P15, although these differences were not statistically significant (one-way ANOVA, df = 2, $p > 0.05$ at all frequencies; Figure 2a). After P15, wave 1 amplitudes in WT mice tended to surpass those of α9KI mice, with significant differences observed at P75 at 16 and 22.65 kHz (one way ANOVA followed by Holm-Sidak test, df=2, p=0.03

at both frequencies; Figure 2a). In α9KO mice, wave 1 amplitudes remained smaller than those of WT and α9KI mice until P16, with the difference being significant only at 22.65 kHz (one way ANOVA followed by Holm-Sidak test, df = 2, p = 0.02; Figure 2a). These findings align with the auditory threshold results, suggesting that the strength of transient MOC efferent innervation to IHCs contributes to the timely development of auditory function. ABR wave 2 amplitudes increased linearly across postnatal ages, stabilizing at P22 in all groups, with no significant differences observed across genotypes at any frequency or age (one way ANOVA, df = 2, p > 0.05 at all frequencies; Figure 2b). Conversely, ABR wave 3 amplitudes showed marked reductions in α9KI mice at most postnatal ages, with significant decreases at P22 and P75 for 16 kHz (one way ANOVA followed by Holm-Sidak test, df = 2, p = 0.005 at P22 and p = 0.01 at P75; Figure 2c). In α9KO mice, reduced wave 3 amplitudes were observed at P15, specifically at 16 kHz (one way ANOVA followed by Holm-Sidak test, df=2, p=0.04; Figure 2c). These findings indicate that both disruption and enhancement of the MOC synapses influence the maturation of cochlear synapses and the development of extra peripheral nuclei in the auditory pathway.

ABR thresholds after early-age noise exposure in mice with different degrees of efferent inhibition

To investigate the impact of early-age noise exposure on auditory development, we exposed WT, α9KO, and α9KI mice to loud noise at P15. At this stage, all three genotypes exhibited measurable ABR waveforms, though their wave 1 thresholds differed and had not yet reached mature levels (Figure 1). This allowed us to evaluate how early noise exposure influences auditory function before threshold maturation in each genotype. Mice were exposed to 1–16 kHz noise at 100 dB SPL for 1 hour at P15. Auditory responses were then assessed at 1, 7, and 60 days post-exposure to track functional changes over time.

Previous studies in WT mice exposed to the same noise protocol at P21 reported significant

auditory threshold shifts of 10–35 dB SPL one day after exposure, with thresholds returning to baseline within a week, indicating a transient threshold shift (31). In contrast, as shown in Figure 3a, no changes in ABR thresholds were observed one day after noise exposure at P16 across frequencies of 8, 16, and 22.65 kHz in WT mice compared to unexposed controls. Remarkably, ABR thresholds at P16 were lower than those measured at P15, prior to noise exposure, suggesting that noise had no immediate impact on the maturation of auditory thresholds at this early postnatal developmental stage. One week after exposure, however, ABR thresholds were elevated at all frequencies in noise-exposed WT animals, and this increase persisted for at least two months post-exposure (Mann- Whitney test, df = 1, P22: $p = 0.006$ at 8 kHz; $p = 0.007$ at 16 kHz; $p = 0.002$ at 22.65 kHz and P75: $p = 0.04$ at 8 kHz; $p = 0.03$ at 16 kHz and $p = 0.04$ at 22.65 kHz; Figure 3a). This outcome contrasts with the transient threshold elevation observed in WT mice, from the same genetic background, exposed at P21 using the same noise protocol (31), suggesting that noise exposure at this early developmental stage produces a more detrimental long-term damage.

A similar trend as seen in WT mice was observed after exposing α9KO mice to noise at P15 (Figure 3b). One day after exposure, there were no changes in ABR thresholds at 8, 16 and 22.65 kHz. However, seven days post-exposure, there was an elevation in auditory thresholds across all frequencies (Mann-Whitney test, df = 1, $p = 0.03$ at 8 kHz; $p = 0.01$ at 16 kHz and $p = 0.02$ at 22.65 kHz), which, unlike in WT mice, returned to normal levels after two months (Mann-Whitney test, df = 1, $p > 0.05$ at all frequencies; Figure 3b). Notably, in α9KI mice, ABR thresholds were not affected by noise exposure at all the frequencies tested (Figure 3c), suggesting that even at this early age, the enhancement of cholinergic activity on OHCs provides protection from noise-induced cochlear threshold elevations (Mann-Whitney test, df = 1, $p > 0.05$ at all frequencies).

Amplitudes of cochlear sound-evoked potentials after early-age noise exposure in mice

with different degrees of efferent inhibition

To assess the neural activity across auditory nerve fibers, we measured ABR wave 1 amplitudes at frequencies of 8, 16, and 22.65 kHz at different ages after noise exposure in the three mouse groups (Figure 4). One day after noise exposure, we observed a reduction in wave 1 amplitudes across all frequencies in WT mice. Further testing WT mice one week and two months post-exposure revealed a significant and lasting reduction, indicating a permanent decrease of ABR wave 1 amplitude (Mann- Whitney test, df = 1, P22: $p = 0.007$ at 8 kHz; $p = 0.005$ at 16 kHz; $p = 0.005$ at 22.65 kHz and P75: $p = 0.04$ at 8 kHz; $p = 0.002$ at 16 kHz and $p = 0.002$ at 22.65 kHz; Figure 4a). Similar permanent reductions in wave 1 amplitude were observed in α9KO mice after exposure to noise at 16 and 22.65 kHz (Mann-Whitney test, df = 1, P22: $p = 0.04$ at 16 kHz; $p = 0.001$ at 22.65 kHz and P75: $p = 0.03$ at 16 kHz and $p = 0.04$ at 22.65 kHz; Figure 4b). Notably, no changes in ABR wave 1 amplitudes were observed at any stage post-exposure in mice with enhanced α9α10 nAChR activity, suggesting a preservation of cochlear synapses after noise exposure (Mann-Whitney test, df = 1, $p > 0.05$ at all frequencies; Figure 4c).

DPOAE thresholds after early-age noise exposure in mice with different levels of α9α10 nAChR activity

To assess the impact of early-age noise exposure on the function of OHCs, we recorded DPOAE at 8, 16, and 22.65 kHz on the three groups of mice with varying levels of MOC function (Figure 5). During early development, the auditory system undergoes significant maturation, leading to decreasing DPOAE thresholds with age, as shown in Figure 1c. In WT mice, one day after noise exposure at P16, there was no difference in DPOAE thresholds between the noise-exposed group and unexposed controls (Figure 5a). Importantly, when comparing DPOAE thresholds at P16 to those at P15 within both groups, a clear reduction was observed (Figure 5a). This decline in thresholds underscores the natural maturation process of the auditory system, indicating that

early noise exposure does not immediately disrupt the ongoing development of DPOAE thresholds at this early postnatal stage. By P22, seven days after noise exposure, an increase in DPOAE thresholds was observed that was statistically significant only at 16 kHz (Mann-Whitney, df = 1, p = 0.01; Figure 5a). Yet, two months later, DPOAE thresholds were comparable to those of unexposed WT controls across all tested frequencies, suggesting that early noise exposure did not result in long-term changes in OHC function (Figure 5a).

In α9KO mice, DPOAE thresholds remained unchanged 1 day after noise exposure. However, significant threshold elevations were observed at 8 and 16 kHz, but not at 22.65 kHz, seven days post-exposure (Mann-Whitney, df = 1, p = 0.02 at 8 kHz and p = 0.02 at 16 kHz). After two months, recovery to unexposed levels occurred only at 8 kHz, while DPOAE thresholds remained elevated at 16 kHz (Mann-Whitney, df = 1, p = 0.003 at 16 kHz; Figure 5b). In contrast, mice with enhanced MOC function showed no changes in DPOAE thresholds at any time point post-exposure (Figure 5c), suggesting that early-age noise exposure did not impair cochlear amplifier function.

Ribbon synapse changes after early noise exposure in mice with different levels of α9α10 nAChR activity

Following the completion of functional testing, histological analysis was performed on cochleae dissected and fixed at P75 from all experimental groups to evaluate the density and structure of IHC ribbon synapses. To visualize these ribbon synapses, we performed immunostaining on whole-mount preparations of the organ of Corti with antibodies against CtBP2-Ribeye, a presynaptic ribbon protein (54), and GluA2, an AMPA-type glutamate receptor expressed at the postsynaptic afferent terminal (30, 55, 56). Ribbon synapses were identified by the colocalization of CtBP2 and GluA2 puncta at the base of the IHC (56). We first compared the number of colocalized synaptic markers per IHC in unexposed WT, α9KO, and α9KI mice across three cochlear locations - apical, medial, and basal - in each cochlear whole-mount (Figure 6). In the

low-frequency apical end, both α9KO and α9KI mice exhibited a significant decrease in synaptic density, with reductions of 30.64% and 27.94%, respectively (Kruskal-Wallis, df=2, $p<0.0001$ for both groups; Figure 6a, left panel). In the medial region, the reduction was significant only in α9KI mice, with a decrease of 35.97% compared to WT (Kruskal-Wallis, df = 2, $p < 0.0001$; Figure 6a, middle panel). Similarly, in the high-frequency basal region, colocalized synaptic puncta were significantly reduced only in α9KI mice, with a 22.07% decrease relative to WT (Kruskal-Wallis, df = 2, $p = 0.02$; Figure 6a, right panel).

We further quantified the volume of CtBP2 puncta and GluA2 receptor patches in these colocalized synaptic markers (Figure 6b, c). In the apical region, both α9KO and α9KI mice showed a reduction in ribbon volumes (one way ANOVA followed by Holm-Sidak test, df = 2, $p < 0.0001$ for both groups; Figure 6b, left panel). In the middle region, the decrease was significant only in α9KI ears in comparison with α9KO ears (one way ANOVA followed by Holm-Sidak test, df = 2, $p < 0.0001$; Figure 6b, middle panel). Interestingly, in the basal region, an increase in CtBP2 volume was detected in α9KO mice, while a decrease was observed in α9KI mice (one way ANOVA followed by Holm-Sidak test, df = 2, $p < 0.0001$ for both groups; Figure 6b, right panel). The size of the GluA2 receptor patches was significantly reduced in α9KI mice in the apical region, with no significant changes in α9KO mice compared to WT (one way ANOVA followed by Holm-Sidak test, df = 2, $p < 0.0001$; Figure 6c, left panel). In the medial region, a reduction in GluA2 volume was observed in both α9KO and α9KI mice (one way ANOVA followed by Holm-Sidak test, df = 2, $p < 0.0001$, for both groups; Figure 6c, middle panel). In the basal region, α9KO mice exhibited an increase in GluA2 size relative to WT (one way ANOVA followed by Holm-Sidak test, df = 2, $p < 0.0001$; Figure 6c, right panel). These results suggest that inhibitory input from cholinergic efferent fibers to hair cells plays a key role in shaping the synaptic density and maintaining the proper morphology of pre- and postsynaptic elements critical for optimal auditory function.

Figure 7 illustrates the impact of early-age noise exposure on auditory nerve synapse numbers across the different experimental groups. Presynaptic, postsynaptic, and colocalized synaptic counts were conducted in the apical, medial, and basal region of the cochlea. In WT exposed ears, the number of presynaptic, postsynaptic, and colocalized synaptic puncta significantly decreased at both the apical and basal cochlear ends (Figure 7a). The reduction in CtBP2 puncta was more pronounced in the high-frequency basal region, showing a 37.2% decrease compared to controls (Mann-Whitney, df = 1, $p < 0.0001$ at the apical and basal regions). Similarly, GluA2 postsynaptic receptors were reduced at both the apical and basal turns in the cochlea of traumatized WT mice (Mann-Whitney, df = 1, $p < 0.0001$ at both cochlear regions). Putative ribbon synapse counts, defined by juxtaposed CtBP2- and GluA2-positive puncta, showed a 34.21% reduction in the apical and a 32.56% reduction in the basal turn following acoustic trauma (Mann-Whitney, df = 1, $p < 0.0001$ at both cochlear regions; Figure 7a, right panel). In α9KO mice, there was also a reduction in the number of presynaptic, postsynaptic, and colocalized puncta depending on cochlear frequency/location after noise exposure (Figure 7b). Ribbon puncta in α9KO exposed ears were reduced by up to 14.73% of the control in the apical and 24.75% in the basal cochlear ends after noise exposure (Mann-Whitney, df = 1, $p = 0.001$ and $p = 0.002$ at the apical and basal region, respectively). GluA2-positive postsynaptic receptor patches decreased by 24.79% in the basal turn of noise-exposed mice (Mann-Whitney, df = 1, $p = 0.004$). Following noise exposure, synaptic puncta were reduced by 26.17% in the apical cochlear region and 25.87% in the basal region (Mann-Whitney, df = 1, $p = 0.002$ and $p < 0.0001$ at the apical and basal region, respectively; Figure 7b, right panel). Interestingly, after two months post-exposure, α9KI ears exhibited no significant changes in presynaptic ribbons, postsynaptic GluA2 receptor patches, or putative synapses across all cochlear regions. Although not statistically significant, a modest increase in synaptic density (~19% at the basal region) was observed in α9KI tissue (Figure 7c, right panel).

We finally quantified the volume of ribbons and AMPA receptor patches at ribbon synapses (i.e., colocalized CtBP2 and GluA2 puncta) from unexposed and exposed mice with different levels of MOC function (Figure 8). In WT mice, noise exposure led to significantly higher ribbon volumes in the basal end of the cochlea compared to unexposed mice, with no corresponding changes in AMPA receptor patch size (t-test, df = 1, p = 0.01; Figure 8 a). No changes were detected in the apical and medial regions of the cochlea (Figure 8 a). Conversely, in α9KO mice, both ribbon and AMPA receptor volumes were reduced in the basal region following noise exposure, while volumes remained unchanged in the apical and medial regions (t-test, df = 1, p = 0.002 for CtbP2 volume and p = 0.003 for GluA2 volume; Figure 8 b). Interestingly, α9KI mice showed no morphological alterations, indicating that enhanced α9α10 nAChR activity protects synapses from noise-induced changes (Figure 8 c).

DISCUSSION

This study examined the influence of MOC inhibitory modulation in auditory maturation and assessed the effects of early loud sound exposure on developmental outcomes. Our findings highlight the importance of the MOC system in the proper establishment of IHC ribbon synapses and reveal that changes in the strength of MOC inhibition impact the timing of hearing onset. Moreover, loud noise exposure during critical developmental stages caused lasting changes in auditory sensitivity in WT, highlighting the greater vulnerability of the auditory system to noise-induced injury during early development. Notably, enhanced cholinergic activity as seen in α9KI mice conferred protection from noise-induced threshold shifts and cochlear synaptopathy. This underscores the crucial protective role of the MOC system during these vulnerable early developmental stages.

Before hearing begins, MOC fibers form direct synapses with IHCs, with cholinergic inhibition playing a key role in regulating the developmental increase in Ca^{2+} sensitivity of glutamate release

at IHC ribbon synapses (18). This regulation is accomplished by precisely modulating IHC action potential activity over a period of immature development (5, 15, 18, 57). It is hypothesized that the maintenance of activity patterns and fidelity in the transmission of these signals are essential for the proper establishment of the sensory map and the refinement of synaptic connections along the auditory pathway (10, 11, 58–61).

The current findings highlight the important role of α9α10 nAChR-mediated activity in auditory function development and ribbon synapse maturation. Enhanced α9α10 nAChR activity in α9KI mice accelerates the onset of hearing, with sound-evoked potentials detected earlier than in mice with normal MOC synapses. Conversely, the absence of MOC activity, as observed in α9KO mice, delays the onset and development of hearing. Consistent with these findings, recent research on α9KO mice has shown that auditory sensitivity at hearing onset is impaired in the absence of pre-hearing efferent input (19). In addition, our work shows that both enhanced and absent MOC inhibition disrupt the normal maturation of ribbon synapses in adult IHCs. Specifically, α9KO and α9KI mice exhibit significant reductions in ribbon synapse density and notable alterations in the volume of pre- and post-synaptic puncta compared to WT mice at P75. This underscores the critical role of balanced MOC activity in auditory system development and synaptic organization. In α9KI mice, enhanced MOC function is associated with reductions in both ribbon size and GluA2 receptor patch volume. Conversely, α9KO mice show region-specific effects: in the apical region of the cochlea, ribbon volume decreases without changes in GluA2 receptor size, whereas in the basal region, both CtBP2 volume and GluA2 receptor size increase. These observations suggest that altered MOC modulation has differential impacts on synaptic structures along the cochlear tonotopic axis. Previous studies have emphasized the functional importance of ribbon size, showing that it is tightly regulated by presynaptic Ca^{2+} channels, with alterations in Ca^{2+} influx impacting synaptic plasticity, neurotransmitter release, and active zone maturation (62–65). During early development, IHC active zones undergo substantial structural and functional

maturation, including the removal of extrasynaptic Ca^{2+} channels and the co-localization of glutamate receptor patches with presynaptic ribbons (66–68). This maturation refines presynaptic morphology, reduces the number of ribbons per synapse, and establishes monosynaptic connections between IHCs and auditory nerve fibers (69–72). Recent work also suggests that fusion of synaptically anchored ribbons during this period is critical for the development of mature active zones and sustained neurotransmitter release (66). Given our observation of reduced ribbon size in some cochlear regions of α9KI and α9KO mice, we propose that altered MOC modulation strength may disrupt intracellular Ca^{2+} dynamics, which could impair ribbon precursor fusion, thereby impairing active zone maturation. These findings highlight the essential role of MOC synapses in shaping early auditory sensitivity and emphasize the importance of coordinated activity between afferent and efferent pathways in regulating spiking activity during this critical developmental window. This coordination is crucial for proper synaptic and auditory system maturation.

Auditory function in vertebrates matures through a well-defined process, transforming the system from high thresholds and limited frequency detection at the onset of hearing to a highly sensitive and precise mechanism capable of resolving frequency differences as small as 1 Hz (73). Our findings suggest that the WT mouse strain used in the present work aligns with this established maturation pattern, as auditory function recordings from P12 to P75 reveal a clear progression from an immature to a mature state. At the onset of hearing (P14 in our strain of mice), the auditory system shows elevated ABR and DPOAE thresholds, reduced wave 1 amplitudes, and poorly defined later ABR waves, reflecting incomplete functional maturation. Over the following days, thresholds progressively decreased, reaching mature levels by P22. This maturation is accompanied by a steady increase in ABR wave 1 amplitudes from P15 to P22, underscoring the critical refinement period necessary for achieving full auditory sensitivity. Thus, by P15, the time when mice were exposed to high levels of noise, the maturation process is not yet complete. A

key finding of this study is that exposure to intense sound during early developmental stages results in significantly more severe consequences compared to exposure at a later age (31). In WT mice, noise exposure at 100 dB SPL for 1 hour at P15 caused persistent ABR threshold elevations lasting up to two months. In contrast, the same exposure at P21 led to only transient threshold shifts, which resolved within seven days (31). This stark difference underscores the heightened vulnerability of the auditory system during early development and highlights the age-dependent impact of noise exposure. Previous reports have also shown that the same scheme of intense noise exposure causes more severe damage in juvenile animals at 4 weeks of age compared to adult animals at 16 weeks of age (74–76). DPOAE thresholds were also elevated seven days post-exposure in WT mice, although these thresholds recovered after two months, suggesting that there is no loss of OHCs or alteration in their function. Given this recovery of DPOAE thresholds but persistently elevated ABR thresholds, we can infer that the elevation is not due to damage in the cochlear amplifier but rather to a deficiency in the afferent pathway of sound signal transmission. In line with this, the increases in ABR thresholds were accompanied by a reduction in the wave 1 amplitude, which also persisted for two months following the exposure to noise. This study represents the first report of sustained ABR threshold elevation for such an extended period following moderate noise exposure at 100 dB SPL for 1 hour. Similar results were obtained in 14-day-old rats exposed to a higher noise level of 125 dB SPL for 25 minutes, where after two months post-exposure, elevated thresholds at high frequencies and a loss of presynaptic elements (CTBP2/Ribeye) were observed (77). In another study involving 10-day-old rats exposed to intense sounds of 105 dB SPL for two hours, a loss of presynaptic elements was also observed after 8 weeks. However, auditory thresholds did not show changes (78). Our findings demonstrate a significant loss of ribbon synapses in the apical and basal regions of the cochlea in WT mice following noise exposure. In addition to cochlear synaptopathy, we observed that IHCs of noise-exposed mice tend to have larger ribbons (Ribeye/CtBP2 volume)

than those of the unexposed IHCs at the basal region of the cochlea. A similar increase in the volume of presynaptic elements following acoustic trauma was observed using both the RIBEYE-tagRFP mouse model (79) and volume electron microscopy (76). The observed ribbon enlargement in WT mice may be attributed to the fusion of individual ribbons after noise exposure. In fact, recent evidence indicates an increase in multi-ribbon active zones as well as movement suggesting unanchoring from synaptic tethers in synaptopathic ears (76, 79, 80). While the functional significance of this structural adaptation remains unclear, multi-ribbon active zones persist into adulthood (66, 67) and are a hallmark of cochlear aging (81), with larger ribbons being associated with increased Ca^{2+}-dependent exocytotic activity (82). Notably, noise exposure has also been associated with enhanced exocytosis in IHCs, along with an increase in tone-burst responses in auditory nerve fibers (83, 84). In addition, studies have shown that intense noise exposure (98 dB SPL for two hours) in young animals reduces the number of presynaptic ribbons in OHCs, while increasing the volume and mobility of the remaining ribbons (85). We can hypothesize that ribbon volume enlargement may act as a compensatory mechanism to maintain auditory sensitivity after synapse loss. Importantly, we did not detect changes in the size of GluA2 receptor patches in WT mice post-noise exposure.

In α9KO mice, which lack α9α10 nAChR activity, elevated ABR and DPOAE thresholds were observed one week after noise exposure at P15, consistent with findings from noise-exposed α9KO mice at P21 (31). However, in contrast to WT animals, ABR thresholds in α9KO mice nearly fully recovered to unexposed control levels two months post-exposure. While DPOAE thresholds returned to control levels at 8 and 22.65 kHz, they remained elevated at 16 kHz after two months. This elevation in DPOAE thresholds at 16 kHz was accompanied by a slight, though not statistically significant, elevation in ABR thresholds at the same frequency. The recovery of ABR thresholds in α9KO mice, compared to the permanent threshold elevation seen in WT mice, may be attributed to the reduced auditory sensitivity at hearing onset in α9KO mice due to the absence

of prehearing efferent modulation. While ABR thresholds return to pre-exposure values, a decrease in wave 1 amplitudes was observed, accompanied by a reduction in the number of ribbon synapses per IHC. Previous work in guinea pigs has suggested that deficits observed post-noise exposure in suprathreshold stimulus encoding are likely due to the preferential impact of noise exposure on high-threshold, low spontaneous firing rate neurons (86). Therefore, we can hypothesize that noise exposure may have specifically affected this particular population of fibers, and thus, despite some degree of synapse loss, changes in ABR thresholds were not observed. However, in α9KO ears exposed to noise, both pre- and postsynaptic puncta showed a reduction in size, indicating noise may also involve maladaptive alterations in both pre- and postsynaptic structures.

In contrast to the findings in WT and α9KO mice, α9KI mice, which exhibit enhanced α9α10 nAChR activity, showed no ABR or DPOAE threshold elevations following sound exposure. Additionally, no evidence of cochlear synaptopathy was detected in these mice. This phenomenon had already been described in adult mice (P21) exposed to the same level of noise (31). At birth, rodent MOC neurons initially innervate IHCs, and by P10, they expand to innervate both IHCs and OHCs. After the onset of hearing, their innervation becomes confined to OHCs, gradually retracting from IHCs (20). Our results therefore suggest that even with early developmental noise exposure—when MOC innervation to OHCs is still developing—enhanced α9α10 nAChR responses can effectively exert a protective effect on OHCs against functional and structural damage associated with acoustic trauma. Importantly, our findings also reveal that mice with enhanced MOC function showed a modest increase in ribbon synapse density following acoustic overexposure. This is consistent with previous work, which documented a more substantial increase in synaptic density in α9KI mice exposed to the same noise protocol at P21 (31). These results indicate that MOC system enhancement may support synapse formation following noise exposure.

In summary, this work highlights three key findings: 1) the MOC system plays a crucial role in regulating the development of ribbon synapse density and size, which is essential for proper hearing onset; 2) early exposure to loud noise results in more severe auditory consequences; and 3) enhancing α9α10 nAChR responses during early development protects against noise-induced damage, underscoring the importance of timely modulation of this receptor post-hearing onset to mitigate developmental impairments.

FIGURES

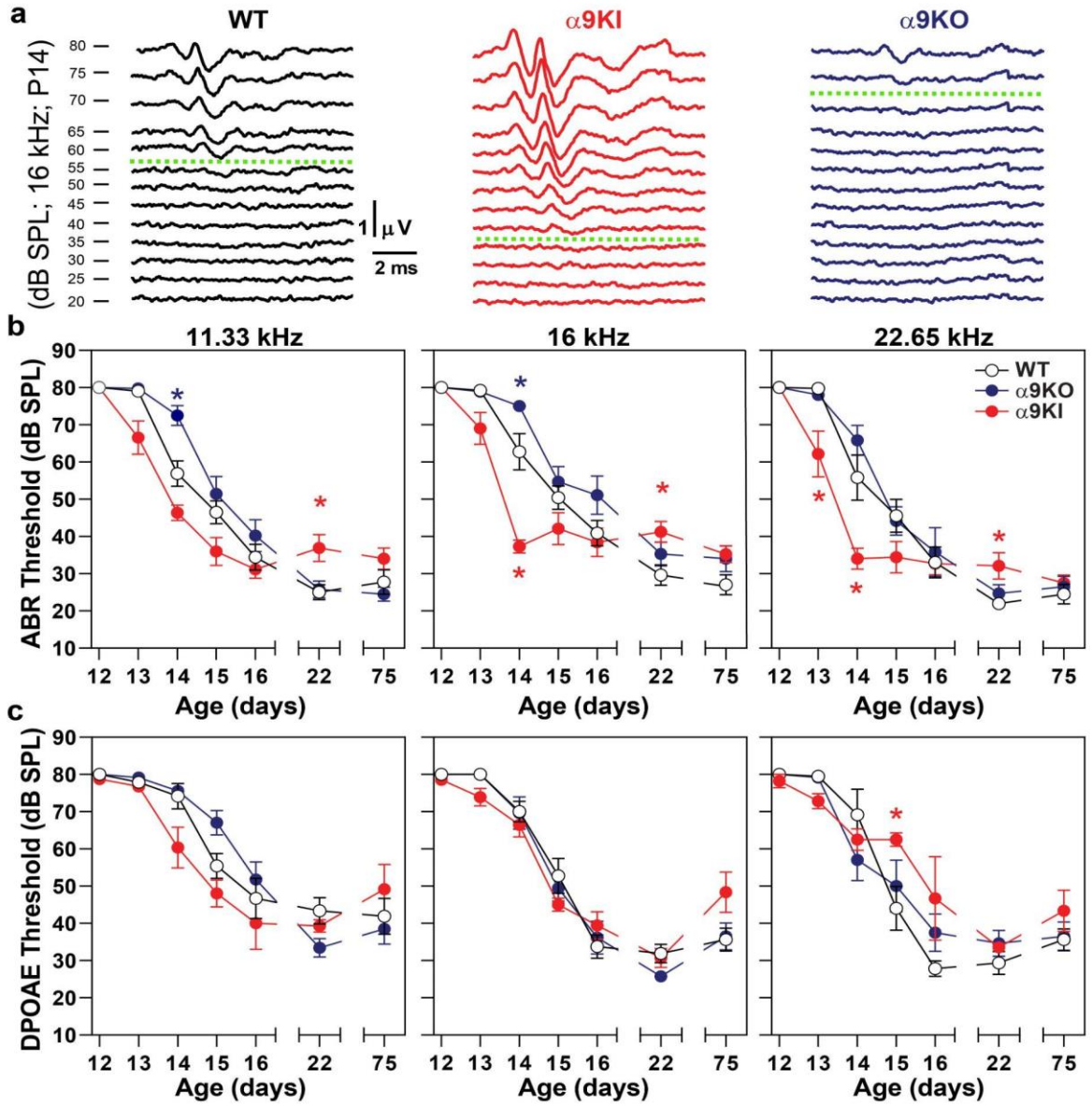

Figure 1: Auditory function in WT, α9KO, and α9KI mice across different postnatal ages. (**a**) Representative ABR waveforms from WT (black), α9KI (red), and α9KO (blue) mice recorded at P14 in response to 16 kHz tone bursts at increasing sound pressure levels (dB SPL). Thresholds, defined by the presence of wave 1, are marked by green dashed traces. The scale bar applies to all three recordings. (**b**) Mean ABR thresholds from P12 to P75 in WT (n = 12), α9KO (n = 14), and α9KI (n = 14) mice at 11.33, 16, and 22.65 kHz. ABR waveforms first became detectable at P13 in α9KI mice, at P14 in WT mice, and between P14 and P15 in α9KO mice. (**c**) Mean DPOAE thresholds from P12 to P75 in WT (n = 12), α9KO (n = 14) and α9KI (n = 14) mice at 11.33, 16 and 22.65 kHz. DPOAE thresholds showed the same trend as ABR only at 11.33 kHz. Group means ± SEM are shown. Red asterisks represent the statistical significance of α9KI compared with WT**,** and blue asterisks represent the statical significance of α9KO compared with WT (Kruskal-Wallis followed by post hoc Dunn test, *p < 0.05).

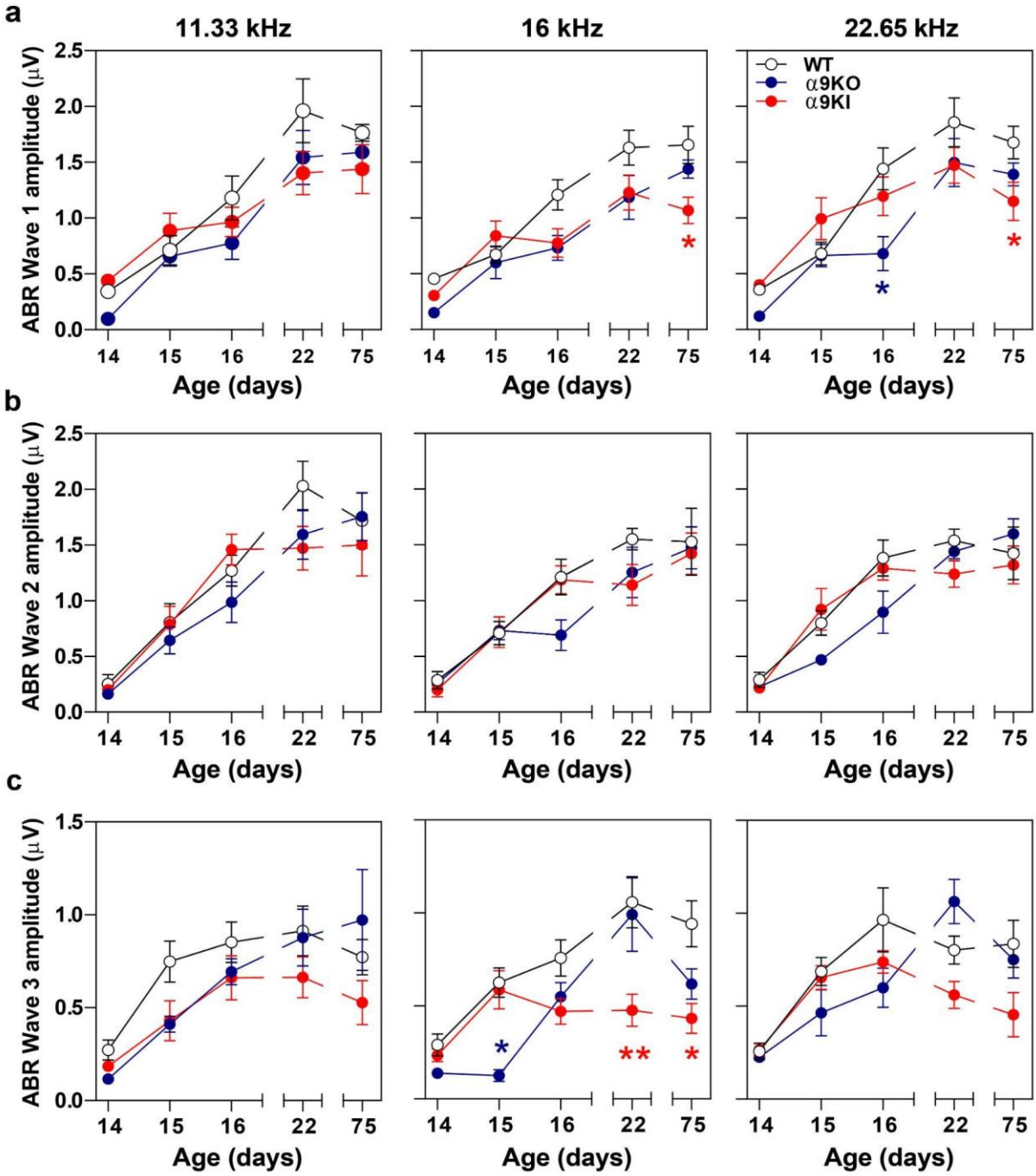

Figure 2: Amplitudes of ABR waves 1, 2, and 3 in WT, α9KO, and α9KI mice across postnatal ages. ABR wave amplitudes (in μV) for waves 1 (**a**), 2 (**b**), and 3 (**c**) in WT, α9KO, and α9KI mice across postnatal ages, measured at 80 dB SPL for frequencies of 11.33, 16, and 22.65 kHz. Amplitudes were determined by calculating the distance between the maximum and minimum peaks. Data points represent the mean ± SEM for WT (n = 12), α9KO (n = 14), and α9KI (n = 14) mice. Red asterisks indicate significant differences between α9KI and WT, while blue asterisks indicate significant differences between α9KO and WT (one-way ANOVA followed by Holm-Sidak test, *p < 0.05; **p < 0.01).

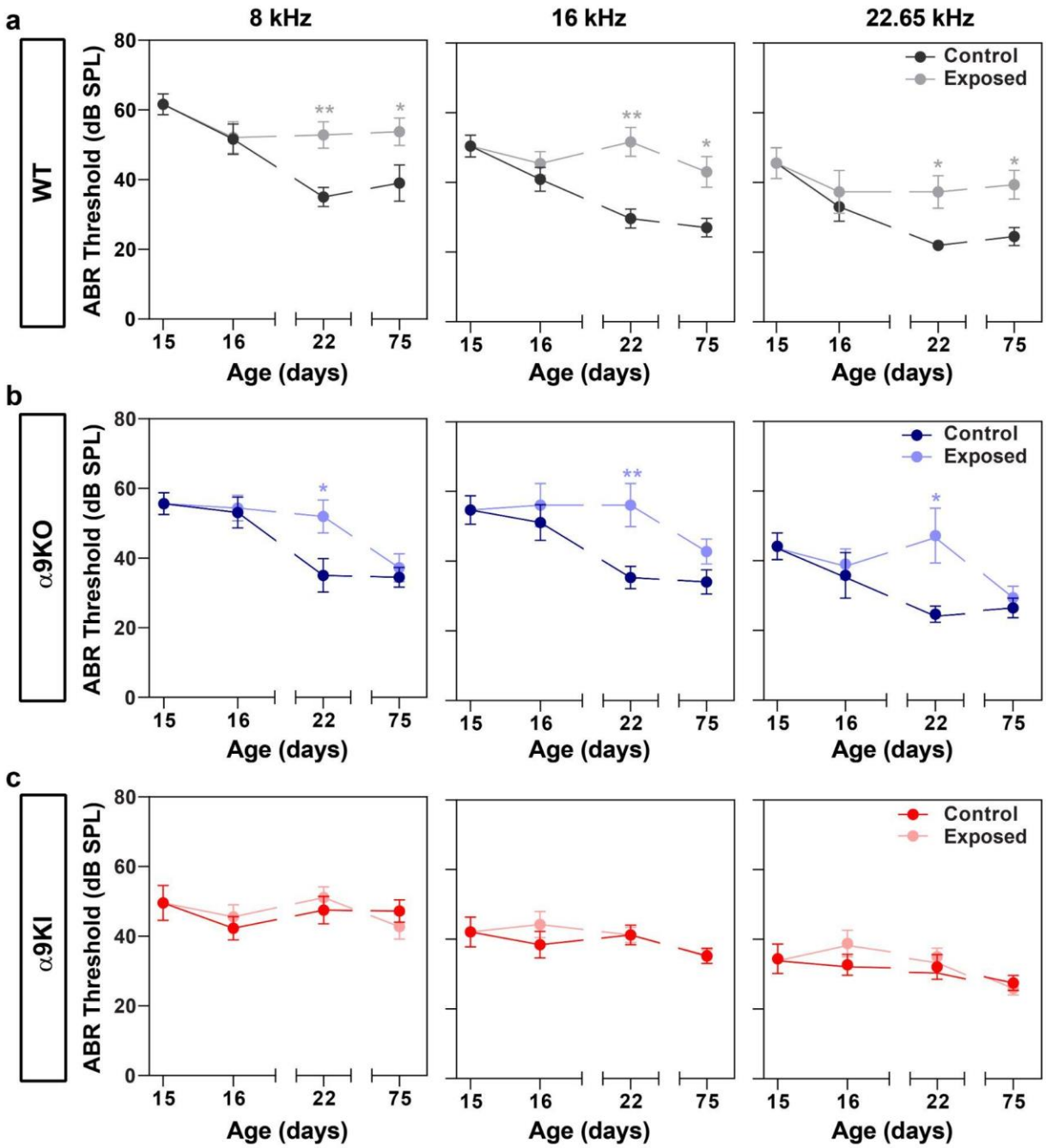

Figure 3: ABR wave 1 threshold measurements in control and noise-exposed WT, α9KO, and α9KI mice at different postnatal ages. ABR thresholds before and after exposure to noise at P15 in WT ($n_{control}$ = 14 and $n_{Exposed}$ = 12) (**a**), α9KO ($n_{control}$ = 11 and $n_{Exposed}$ = 11) (**b**), and α9KI ($n_{control}$ = 12 and $n_{Exposed}$ = 12) (**c**) mice at 8, 16 and 22.65 kHz. WT mice showed a significant increase in ABR thresholds 1 week and 2 months after exposure to noise, indicating a permanent threshold elevation. A recovery of ABR thresholds was observed in α9KO mice 2 months after exposure to noise. α9KI mice did not present any changes in ABR thresholds at any time after acoustic trauma. Each point represents the mean ± SEM. Asterisks represent the statistical significance (Mann-Whitney test, *$p < 0.05$; **$p < 0.01$).

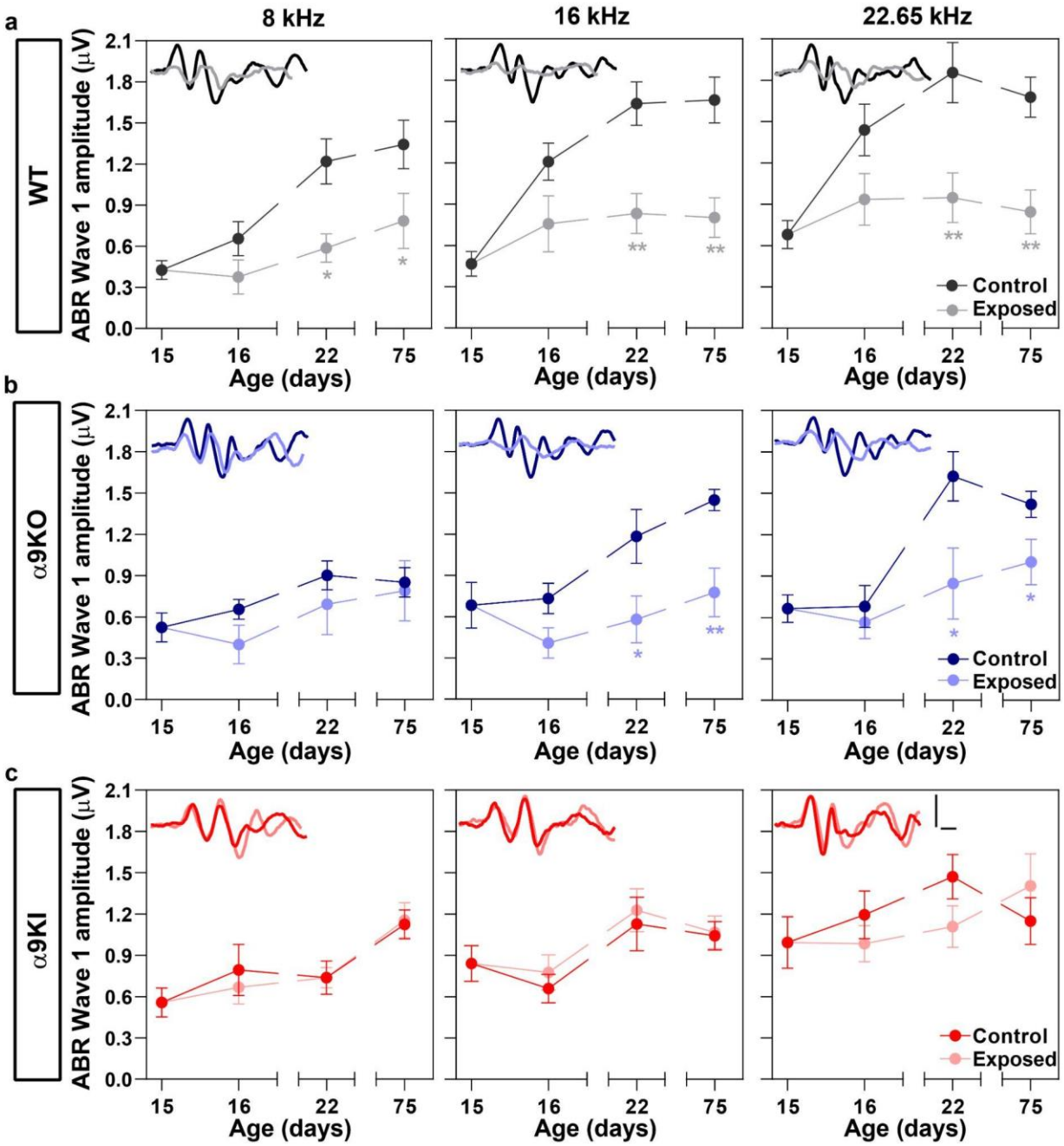

Figure 4: Suprathreshold response amplitude for ABR wave 1 after P15 noise exposure in WT, α9KO, and α9KI mice at different postnatal ages compared to unexposed controls. ABR wave 1 amplitudes (in μV) at 80 dB SPL at 8, 16 and 22.65 kHz in WT ($n_{Control}$ = 14 and $n_{Exposed}$ = 12) (**a**), α9KO ($n_{Control}$ = 11 and $n_{Exposed}$ = 11) (**b**), and α9KI ($n_{Control}$ = 12 and $n_{Exposed}$ = 12) (**c**) mice at the same time points shown in Figure 3. Each panel inset displays representative ABR waveforms recorded at 80 dB SPL for the corresponding frequency, shown for all groups at P75. Scale bars (1 μV vertical, 1 ms horizontal) apply to all traces. WT and α9KO mice exhibited reduced ABR wave 1 amplitudes following noise exposure, whereas wave 1 amplitudes in α9KI mice remained unaffected. Data are presented as mean ± SEM. Statistical significance is indicated by asterisks (Mann-Whitney test, *$p < 0.05$; **$p < 0.01$).

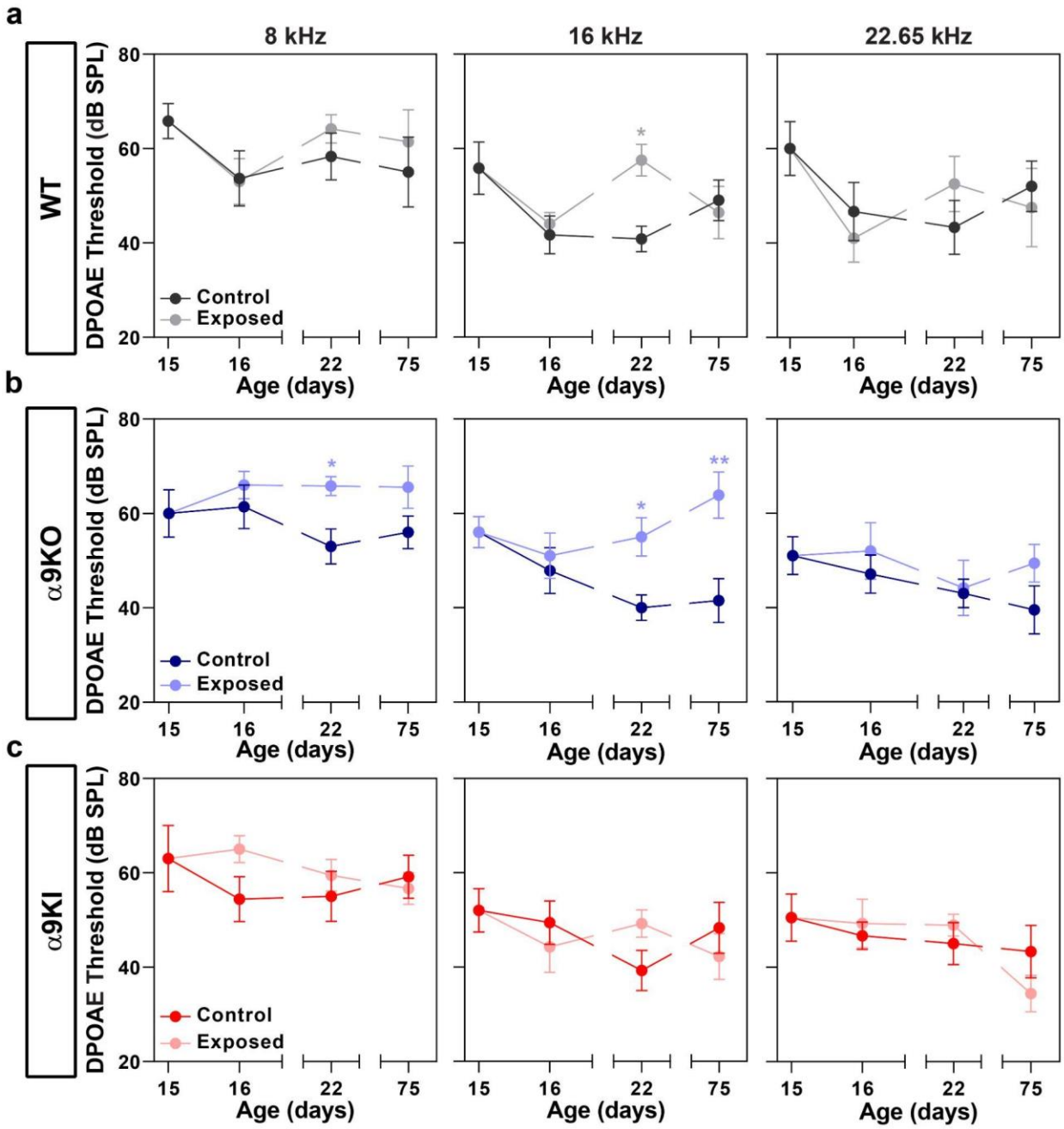

Figure 5: **Assessment of OHC functional integrity at different postnatal ages following noise exposure at P15 in WT, α9KO, and α9KI mice.** DPOAE thresholds are shown for WT ($n_{Control}$ = 14 and $n_{Exposed}$ = 12) (**a**), α9KO ($n_{Control}$ = 11 and $n_{Exposed}$ = 11) (**b**), and α9KI ($n_{Control}$ = 12 and $n_{Exposed}$ = 12) (**c**) at 8, 16 and 22.65 kHz. WT mice exhibited a transient increase in DPOAE thresholds 1 week post-exposure at 16 kHz. α9KO mice showed increased thresholds at 8 and 16 kHz 1 week post-exposure, with sustained elevation at 16 kHz up to 2 months. α9KI mice demonstrated no changes in DPOAE thresholds after noise exposure. Data are presented as mean ± SEM. Statistical significance is indicated by asterisks (Mann-Whitney test, *$p < 0.05$; **$p < 0.01$).

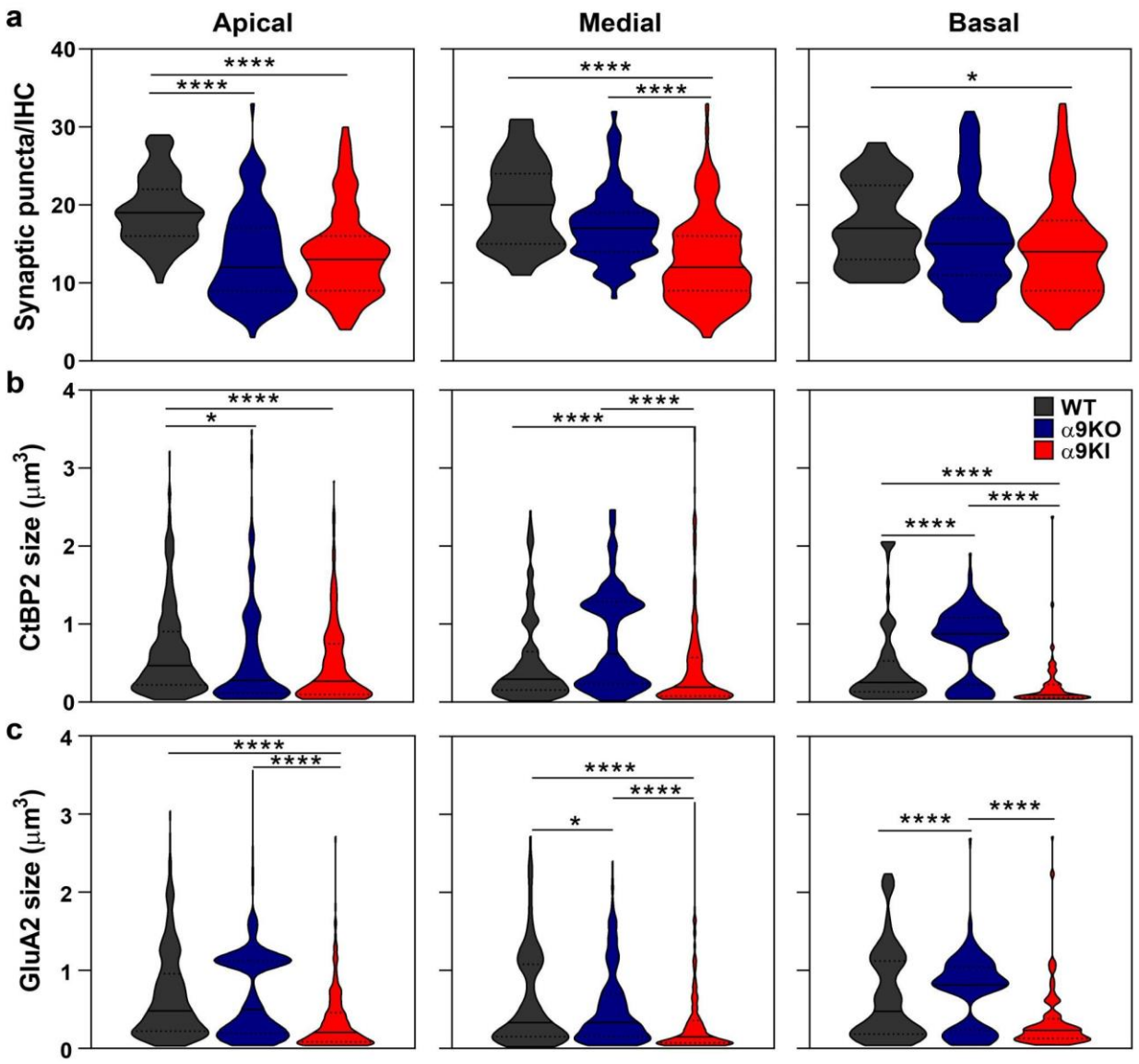

Figure 6: Analysis of IHC ribbon synapses in unexposed WT, α9KO, and α9KI mice. Quantitative data obtained from unexposed mice at P75 at the apical (left panel), medial (middle panel) and basal cochlear region (right panel). (**a**) Number of putative ribbon synapses per IHC (i.e., colocalized CtBP2 and GluA2 puncta). WT: n_{Apical} = 80 IHC, n_{Medial} = 75 IHC, n_{Basal} = 60 IHC from 14 animals; α9KO: n_{Apical} = 100 IHC, n_{Medial} = 84 IHC, n_{Basal} = 118 IHC from 11 animals and α9KI: n_{Apical} = 178 IHC, n_{Medial} = 319 IHC, n_{Basal} = 198 IHC from 12 animals. (**b**) Volumes of fluorescence staining for ribbons (CtBP2 size) and (**c**) AMPA receptors (GluA2 size) for each of the synaptic pairs (WT: n_{Apical} = 450 synaptic pairs, n_{Medial} = 509 synaptic pairs, n_{Basal} = 203 synaptic pairs; α9KO: n_{Apical} = 367 synaptic pairs, n_{Medial} = 187 synaptic pairs, n_{Basal} = 221 synaptic pairs and α9KI: n_{Apical} = 247 synaptic pairs, n_{Medial} = 270 synaptic pairs, n_{Basal} = 240 synaptic pairs). Violin plots indicate median (solid line) and interquartile range (IQR, dashed lines). Asterisks denote the statistical significance (Kruskal–Wallis followed by a Dunn's post-test was used to analyze the number of synapses and one way ANOVA followed by Holm-Sidak test; *$p < 0.05$; **$p < 0.01$; ***$p < 0.001$, ****$p < 0.0001$).

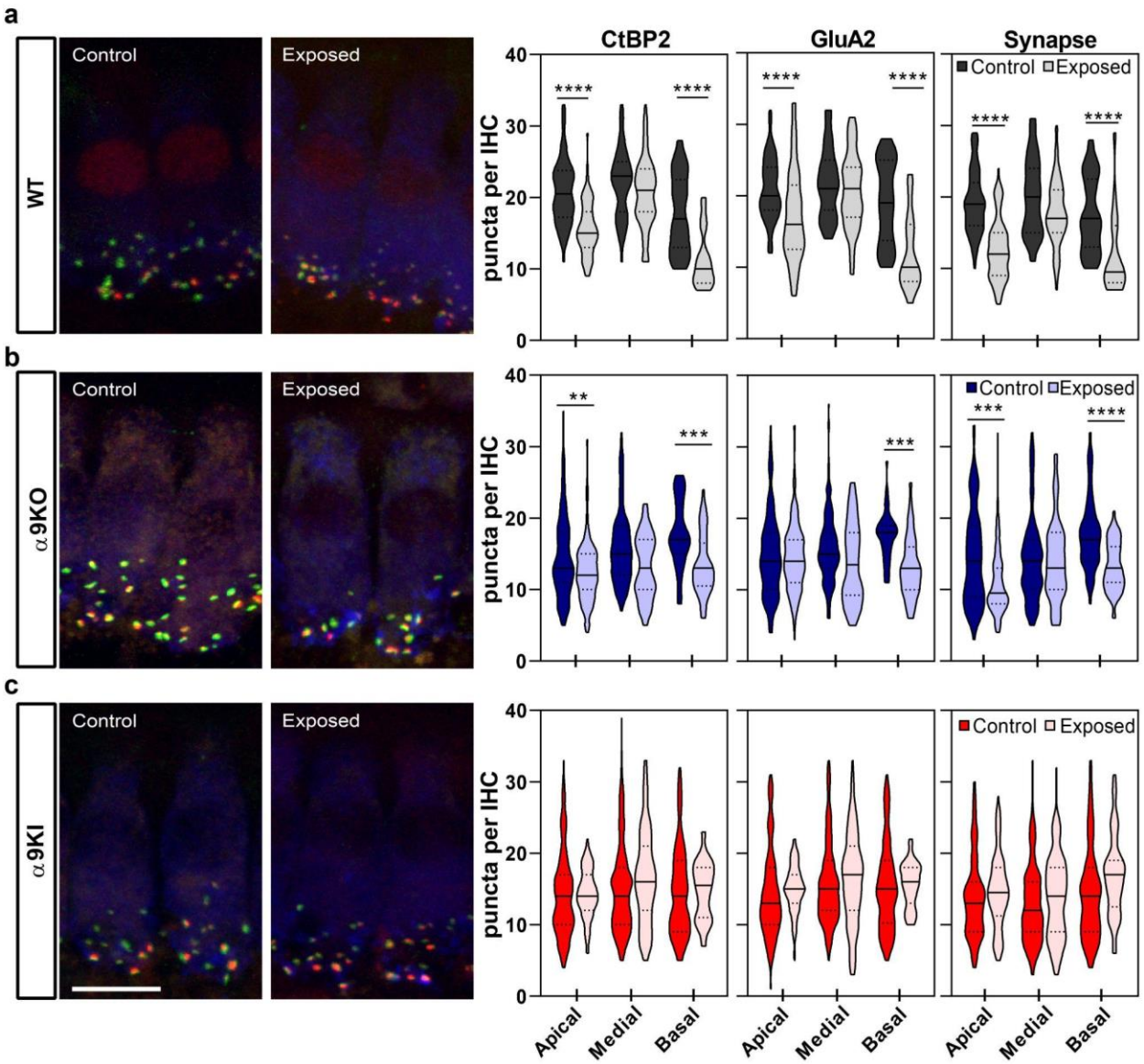

Figure 7: Analysis of the degree of IHC synaptopathy two months after exposure to noise at P15. Left, Representative confocal images of IHC synapses at the apical region from cochleae immunolabeled for presynaptic ribbons (CtBP2-red), postsynaptic receptor patches (GluA2-green) and IHCs (Myosin VIIa-blue). CtBP2 antibody also weakly stains IHC nuclei. Scale bar, 10μm. Right, Quantitative data obtained from WT, α9KO, and α9KI mice at P75. For each IHC, we analyzed the number of CtBP2 puncta, postsynaptic GluA2 receptor patches, and putative ribbon synapses. (**a)** In traumatized WT mice, there was a reduction in the number of CtBP2 puncta, GluA2 receptor patches, and putative synapse, at the apical and basal region of the cochlea (WT Control: n_{Apical} = 80 IHC, n_{Medial} = 75 IHC, n_{Basal} = 60 IHC; WT Exposed: n_{Apical} = 82 IHC, n_{Medial} = 90 IHC, n_{Basal} = 50 IHC). (**b**) In traumatized α9KO mice, there was a reduction in the number of prelocalized, postlocalized, and colocalized puncta depending on cochlear frequency/location (α9KO Control: n_{Apical} = 100 IHC, n_{Medial} = 84 IHC, n_{Basal} = 118 IHC; α9KO Exposed: n_{Apical} = 234 IHC, n_{Medial} = 60 IHC, n_{Basal} = 90 IHC). (**c**) In traumatized α9KI mice, no

difference was found in the number of presynaptic ribbons, postsynaptic AMPA receptors, and colocalization puncta for the three regions of the cochlea (α9KI Control: n_{Apical} = 178 IHC, n_{Medial} = 319 IHC, n_{Basal} = 198 IHC; α9KI Exposed: n_{Apical} = 196 IHC, n_{Medial} = 145 IHC, n_{Basal} = 80 IHC). Violin plots indicate median (solid line) and IQR (dashed lines). Asterisks denote the statistical significance (Mann Whitney test, **$p < 0.01$; ***$p < 0.001$, ****$p < 0.0001$).

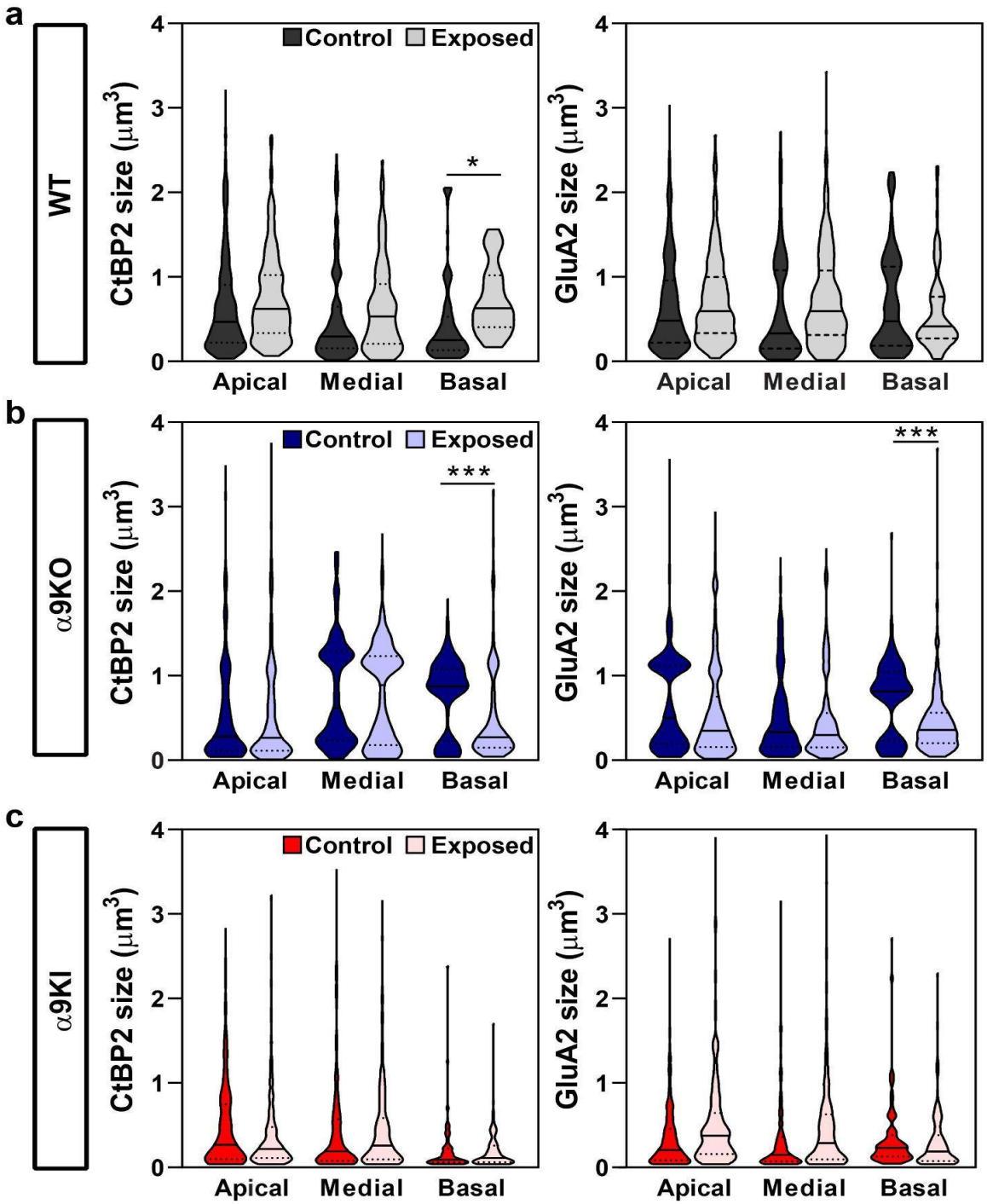

Figure 8: Volumes of presynaptic ribbons and postsynaptic receptor patches for each synaptic pair from control and noise-exposed WT, α9KO and α9KI mice. Violin plots comparing the volumes of fluorescence staining for ribbons (CtBP2 size) and AMPA receptors (GluA2 size) between control and noise-exposed mice. The quantification was made at the apical, medial and basal cochlear regions from WT (**a**) (Control: n_{Apical} = 450 synaptic pairs, n_{Medial} = 509 synaptic pairs, n_{Basal} = 203 synaptic pairs; Exposed: n_{Apical} = 497 synaptic pairs, n_{Medial} = 175

synaptic pairs, n_{Basal} = 250 synaptic pairs); α9KO (**b**) (Control: n_{Apical} = 367 synaptic pairs, n_{Medial} = 187 synaptic pairs, n_{Basal} = 221 synaptic pairs; Exposed: n_{Apical} = 207 synaptic pairs, n_{Medial} = 300 synaptic pairs, n_{Basal} = 145 synaptic pairs) and α9KI (**c**) (Control: n_{Apical} = 247 synaptic pairs, n_{Medial} = 270 synaptic pairs, n_{Basal} = 240 synaptic pairs; Exposed: n_{Apical} = 280 synaptic pairs, n_{Medial} = 310 synaptic pairs, n_{Basal} = 360 synaptic pairs) mice. Violin plots indicate median (solid line) and IQR (dashed lines). Asterisks denote the statistical significance (t-test; *$p < 0.05$; ***$p < 0.001$).

SUPPLEMENTAL INFORMATION

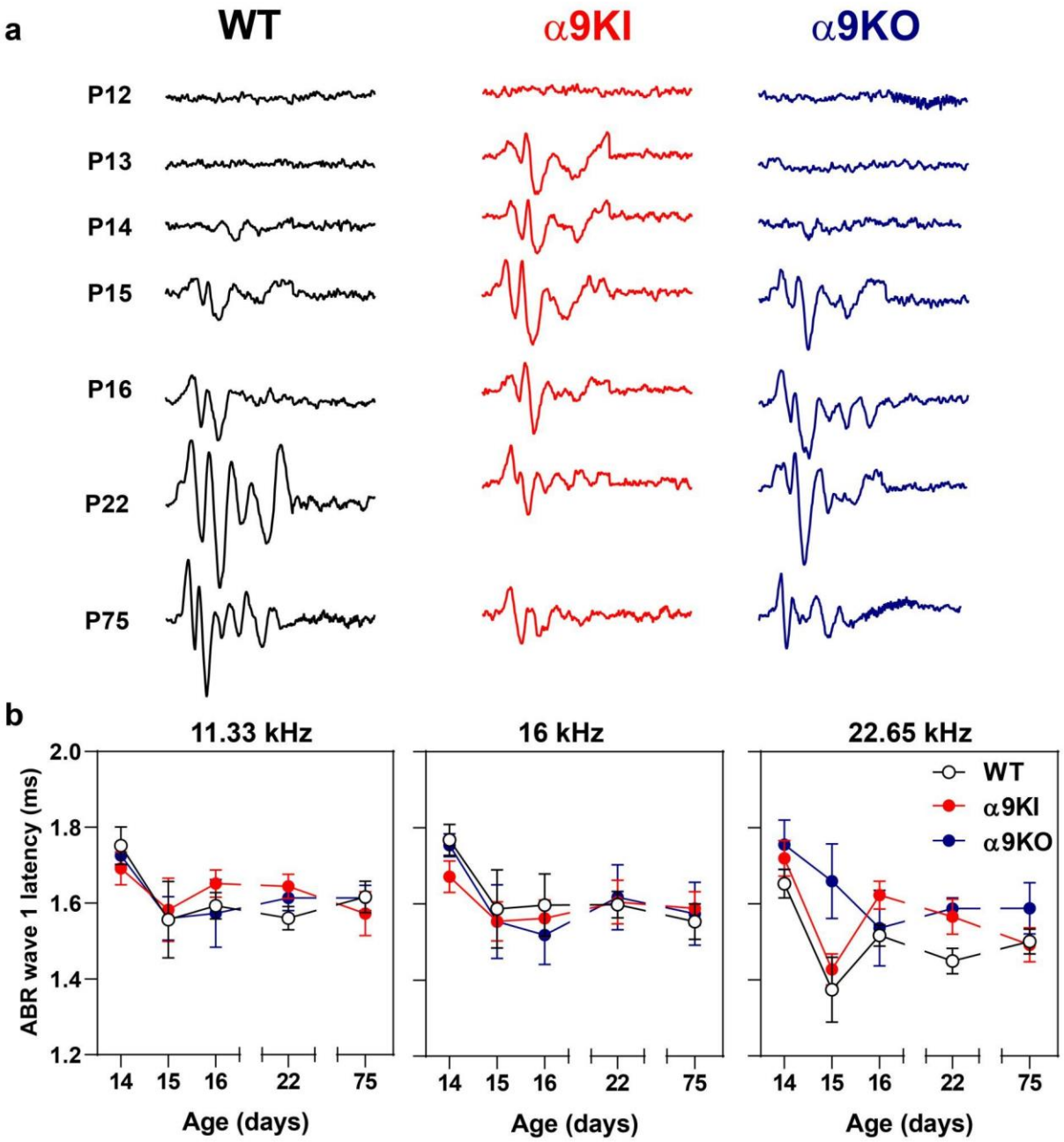

Supplementary Figure 1. Suprathreshold ABR waveforms and wave 1 latencies in WT, α9KO, and α9KI mice across postnatal development. (**a**) Representative ABR traces at 16 kHz, 80 dB SPL, from WT (black), α9KI (red), and α9KO (blue) mice, recorded at P12–P16, P22, and P75. At P13, α9KI mice exhibit measurable responses, whereas distinct ABR waves emerge in WT and α9KO mice by P14. By P22, ABR amplitudes stabilize and remain consistent through P75. Scale bar applies to all traces. (**b**) ABR wave 1 latencies at 11.33, 16, and 22.65 kHz for WT, α9KI, and α9KO mice. All groups show a reduction in latency between P14 and P15, though this change is not statistically significant. Data are shown as mean ± SEM.

METHOD DETAILS

Animals. α9KO and α9KI mice have been previously described (29, 45) and were backcrossed with the congenic FVB.129P2-*Pde6bþ Tyrc-ch/AntJ* strain (https://www.jax.org/strain/004828) for seventeen generations (i.e., N-17). We maintained a consistent male-to-female ratio across all experimental groups and genotypes. No sex-related differences were observed in the data. Animals were housed in a sound-controlled room within the animal care facility. Background sound levels in this environment were consistently below 50 dB SPL. Noise levels were measured using an electret condenser microphone (FG-23329-PO7; Knowles). Transient sounds during routine cage cleaning and daily maintenance by animal care staff were minimal, with peaks not exceeding 70 dB SPL. The methods reported in this study adhere to the ARRIVE guidelines for reporting *in vivo* animal research (https://arriveguidelines.org/), ensuring transparency and reproducibility. All procedures were conducted in accordance with institutional and ethical guidelines for animal care and use.

Auditory function tests. Physiological assessments of cochlear and central function, including auditory brainstem responses (ABRs) and distortion-product otoacoustic emissions (DPOAEs), were performed in mice anesthetized with xylazine (10 mg/kg, i.p.) and ketamine (100 mg/kg, i.p.) and placed in a soundproof chamber maintained at 32°C to counteract the drop in body temperature caused by anesthesia. ABR represents sound-evoked potentials generated by neural circuits in the ascending auditory pathways, while DPOAEs are sounds emitted by the cochlea, specifically by OHCs, in response to two pure-tone stimuli presented simultaneously. Sound stimuli were delivered through a custom acoustic system with two dynamic earphones used as sound sources (CDMG15008–03A; CUI) and an electret condenser microphone (FG-23329-PO7; Knowles) coupled to a probe tube to measure sound pressure near the eardrum. Data collection was conducted using a National Instruments PXI-based system equipped with 24-

bit input/output boards and operated through a custom LabView software interface. For ABRs, platinum needle electrodes were placed into the skin at the dorsal midline close to the neural crest and pinna with a ground electrode near the tail. ABR potentials were evoked with 5 ms tone pips (0.5 ms rise-fall, with a $\cos^2$ envelope, at 40/s) delivered to the eardrum at log-spaced frequencies from 5.6 to 45.25 kHz. The response was amplified 10,000X with a 0.3–3 kHz passband. Sound level was raised in 5 dB steps from 20 to 80 dB sound pressure level (SPL). At each level, 1024 responses were averaged with alternated stimulus polarity. Threshold for ABR was defined as the lowest stimulus level (<80 dB SPL) at which a repeatable wave 1 could be identified in the response waveform. The ABR waves 1, 2 and 3 amplitudes were computed by off-line analysis of the peak-to-peak amplitude of stored waveforms. The DPOAEs in response to two primary tones of frequency f1 and f2 were recorded at 2f1-f2, with f2/f1=1.2, and the f2 level 10 dB lower than the f1 level. Ear-canal sound pressure was amplified and digitally sampled at 4 µs intervals. DPOAE threshold was defined as the lowest f2 level in which the signal to noise floor ratio is >1.

Noise exposure. Animals were exposed under anesthesia at P15 to a 1–16 kHz noise at 100 dB SPL for 1 hour using closed-field earphones (CDMG15008–03A; CUI) as the sound source. The exposure took place in the same acoustic chamber used for cochlear function tests. The noise consisted of a flat-spectrum broadband signal calibrated to the target SPL immediately before each exposure session.

Cochlear processing and immunostaining. Cochleae were perfused intralabyrinthly with 4% paraformaldehyde (PFA) in phosphate-buffered saline (PBS), post-fixed with 4% PFA overnight, and decalcified in 0.12 M EDTA. Cochlear tissues were then microdissected and permeabilized by freeze/thawing in 30% sucrose. The microdissected pieces were blocked in 5% normal goat serum with 1% Triton X-100 in PBS for 1 h, followed by incubation in primary antibodies (diluted

in blocking buffer) at 37°C for 16 h. The primary antibodies used in this study were: 1) anti-C-terminal binding protein 2 (mouse anti-CtBP2 IgG1; BD Biosciences, San Jose, CA; Cat#612044, RRID:AB_399431, 1:200) to label the presynaptic ribbon, 2) anti-glutamate receptor 2 (mouse anti-GluA2 IgG2a; Millipore, Billerica, MA; Cat#MAB397, RRID:AB_11212990, 1:2000) to label the post-synaptic receptor plaques and 3) anti-Myosin 7a (rabbit anti-MyosinVIIa, Proteus Biosciences; Cat# 25-6790, RRID:AB_10015251, 1:200) to label the cochlear hair cells. Tissues were then incubated with the appropriate Alexa Fluor-conjugated fluorescent secondary antibodies (Invitrogen, Carlsbad, CA; 1:500 in blocking buffer) for 2 hours at room temperature. Finally, tissues were mounted on microscope slides in FluorSave mounting media (Millipore, Billerica, MA).

Confocal microscopy and image processing. For IHC synaptic counts, confocal z-stacks (0.3 µm step size) of the apical, medial and basal regions from each cochlea were taken using a Leica TCS SPE microscope equipped with 63X (1.5X or 4X digital zoom) oil-immersion lens. Each stack usually contained 10 to 20 IHCs. Image stacks were imported to Fiji software (RRID:SCR_002285) (87) and a custom plugin was developed to automate the counting of synaptic ribbons, glutamate receptor patches and co-localized synaptic puncta. The algorithm's accuracy was validated by comparing automated counts to manual counts, ensuring reliable quantification. Briefly, each channel was analyzed separately, and maximum projections were generated to quantify the number of CtBP2 or GluA2 puncta. Additionally, a composite between the three channels was produced to draw the different regions of interest (ROI) that correspond to each IHC taking the myosin staining as a reference. The maximum projections from the single channels were multiplied to generate a merged 32-bit image. Then, they were converted to binary images after a custom thresholding procedure. An automatic counting of the number of particles on each ROI was performed.

For quantitative volumetric synaptic analysis, different regions from the whole cochlea were imaged and confocal z-stacks were processed in Fiji. z-stacks were deconvolved applying 10 iterations of the Richardson-Lucy algorithm in the DeconvolutionLab2 plugin (88), an algorithm that has been used previously in cochlear whole mounts (89). Then, the 3D Object Counter plugin was used to perform three-dimensional image segmentation and object individualization of the deconvoluted stacks. According to previous work (56, 90, 91) we reasoned that a synapse would occupy a volume between 0.04 µm3 to 5 µm3, and then we set a size range of 20-2000 voxels, with a voxel size of 0.11 µm x 0.11 µm x 0.2 µm. The volumes of presynaptic ribbons (CtBP2 fluorescence) and postsynaptic AMPA receptor clusters (GluA2 fluorescence) at IHC-afferent synapses were measured using the 3D ROI Manager (92). All exported volumes were checked to ensure that volumes were within instrument resolution limits after threshold adjustments.

Statistical analysis

Data were analyzed using R Statistical Software (RRID:SCR_001905). Shapiro-Wilks test was used for testing normal distribution of the residuals. In cases where the data did not follow a normal distribution, the following tests were used: Kruskal-Wallis test followed by multiple contrasts according to Dunn's method for comparisons between three groups (IHCs synaptic counts in the control condition) and Mann-Whitney U test for comparisons between two groups (ABR thresholds, DPOAE thresholds, and IHCs synaptic counts). If data were normally distributed, a one-way ANOVA was conducted, followed by Holm-Sidak post hoc tests for three-group comparisons (wave 1 amplitudes and synaptic volumes in the control condition). For two-group comparisons, a t-test was used (synaptic volumes). Statistical significance was set to $p<0.05$.

REFERENCES

1. W. R. Lippe, Rhythmic spontaneous activity in the developing avian auditory system. *J Neurosci* **14**, 1486–1495 (1994).

2. W. Marcotti, S. L. Johnson, A. Rusch, C. J. Kros, Sodium and calcium currents shape action potentials in immature mouse inner hair cells. *J Physiol* **552**, 743–761 (2003).

3. M. Sonntag, B. Englitz, C. Kopp-Scheinpflug, R. Rübsamen, Early Postnatal Development of Spontaneous and Acoustically Evoked Discharge Activity of Principal Cells of the Medial Nucleus of the Trapezoid Body: An In Vivo Study in Mice. *J. Neurosci.* **29**, 9510–9520 (2009).

4. N. X. Tritsch, D. E. Bergles, Developmental regulation of spontaneous activity in the Mammalian cochlea. *J. Neurosci. Off. J. Soc. Neurosci.* **30**, 1539–1550 (2010).

5. S. L. Johnson, *et al.*, Position-dependent patterning of spontaneous action potentials in immature cochlear inner hair cells. *Nat. Neurosci.* **14**, 711–717 (2011).

6. T. S. Tierney, F. A. Russell, D. R. Moore, Susceptibility of developing cochlear nucleus neurons to deafferentation-induced death abruptly ends just before the onset of hearing. *J. Comp. Neurol.* **378**, 295–306 (1997).

7. E. Friauf, C. Lohmann, Development of auditory brainstem circuitry. Activity-dependent and activity-independent processes. *Cell Tissue Res.* **297**, 187–195 (1999).

8. S. P. Mostafapour, S. L. Cochran, N. M. Del Puerto, E. W. Rubel, Patterns of cell death in mouse anteroventral cochlear nucleus neurons after unilateral cochlea removal. *J. Comp. Neurol.* **426**, 561–571 (2000).

9. P. A. Leake, G. T. Hradek, L. Chair, R. L. Snyder, Neonatal deafness results in degraded topographic specificity of auditory nerve projections to the cochlear nucleus in cats. *J. Comp. Neurol.* **497**, 13–31 (2006).

10. A. Clause, *et al.*, The precise temporal pattern of prehearing spontaneous activity is necessary for tonotopic map refinement. *Neuron* **82**, 822–835 (2014).

11. M. N. Di Guilmi, *et al.*, Strengthening of the efferent olivocochlear system leads to synaptic dysfunction and tonotopy disruption of a central auditory nucleus. *J. Neurosci.* 2536–18 (2019). https://doi.org/10.1523/jneurosci.2536-18.2019.

12. W. Marcotti, S. L. Johnson, M. C. Holley, C. J. Kros, Developmental changes in the expression of potassium currents of embryonic, neonatal and mature mouse inner hair cells. *J Physiol* **548**, 383–400 (2003).

13. H. C. Wang, *et al.*, Spontaneous Activity of Cochlear Hair Cells Triggered by Fluid Secretion Mechanism in Adjacent Support Cells. *Cell* **163**, 1348–1359 (2015).

14. S. L. Johnson, J. Olt, S. Cho, H. von Gersdorff, W. Marcotti, The Coupling between Ca^{2+} Channels and the Exocytotic Ca^{2+} Sensor at Hair Cell Ribbon Synapses Varies Tonotopically along the Mature Cochlea. *J. Neurosci.* **37**, 2471–2484 (2017).

15. E. Glowatzki, P. A. Fuchs, Cholinergic synaptic inhibition of inner hair cells in the neonatal mammalian cochlea. *Science* **288**, 2366–68 (2000).

16. W. Marcotti, S. L. Johnson, C. J. Kros, A transiently expressed SK current sustains and modulates action potential activity in immature mouse inner hair cells. *J Physiol* (2004).

17. J. D. Goutman, P. A. Fuchs, E. Glowatzki, Facilitating efferent inhibition of inner hair cells in the cochlea of the neonatal rat. *J. Physiol.* **566**, 49–59 (2005).

18. S. L. Johnson, *et al.*, Cholinergic efferent synaptic transmission regulates the maturation of auditory hair cell ribbon synapses. *Open Biol.* **3** (2013).

19. Y. Wang, *et al.*, Efferent feedback controls bilateral auditory spontaneous activity. *Nat. Commun.* **12**, 2449 (2021).

20. D. D. Simmons, N. B. Mansdorf, J. H. Kim, Olivocochlear innervation of inner and outer hair cells during postnatal maturation: evidence for a waiting period. *J Comp Neurol* **370**, 551–562 (1996).

21. L. G. Vattino, C. Wedemeyer, A. B. Elgoyhen, E. Katz, Functional Postnatal Maturation of the Medial Olivocochlear Efferent–Outer Hair Cell Synapse. *J. Neurosci.* **40**, 4842–4857 (2020).

22. J. J. Guinan, P. Dallos, A. N. Popper, R. R. Fay, “Efferent Physiology” in *The Cochlea*, P. Dallos, A. N. Popper, R. R. Fay, Eds. (Springer, 1996), pp. 435–502.

23. R. L. Winslow, M. B. Sachs, Effect of electrical stimulation of the crossed olivocochlear bundle on auditory nerve response to tones in noise. *J. Neurophysiol.* **57**, 1002–1021 (1987).

24. R. L. Winslow, M. B. Sachs, Single-tone intensity discrimination based on auditory-nerve rate responses in backgrounds of quiet, noise, and with stimulation of the crossed olivocochlear bundle. *Hear Res* **35**, 165–189 (1988).

25. T. Kawase, M. C. Liberman, Antimasking effects of the olivocochlear reflex. I. Enhancement of compound action potentials to masked tones. *J Neurophysiol* **70**, 2519–2532 (1993).

26. P. H. Delano, D. Elgueda, C. M. Hamame, L. Robles, Selective attention to visual stimuli reduces cochlear sensitivity in chinchillas. *J Neurosci* **27**, 4146–4153 (2007).

27. M. C. Liberman, The olivocochlear efferent bundle and susceptibility of the inner ear to acoustic injury. *J Neurophysiol* **65**, 123–132 (1991).

28. S. F. Maison, M. C. Liberman, Predicting Vulnerability to Acoustic Injury with a Noninvasive Assay of Olivocochlear Reflex Strength. *J. Neurosci.* **20**, 4701–4707 (2000).

29. J. Taranda, *et al.*, A point mutation in the hair cell nicotinic cholinergic receptor prolongs cochlear inhibition and enhances noise protection. *PLoS Biol.* **7**, 71–83 (2009).

30. S. F. Maison, H. Usubuchi, M. C. Liberman, Efferent feedback minimizes cochlear neuropathy from moderate noise exposure. *J. Neurosci.* **33**, 5542–5552 (2013).

31. L. E. Boero, *et al.*, Enhancement of the medial olivocochlear system prevents hidden hearing loss. *J. Neurosci.* **38**, 7440–7451 (2018).

32. C. M. Liberman, L. D. Liberman, S. F. Maison, Efferent feedback slows cochlear aging. *J. Neurosci.* **34**, 4599–4607 (2014).

33. L. E. Boero, *et al.*, Preventing presbycusis in mice with enhanced medial olivocochlear feedback. *Proc Natl Acad Sci U A* **117**, 11811–11819 (2020).

34. E. F. Chang, M. M. Merzenich, Environmental noise retards auditory cortical development. *Science* **300**, 498–502 (2003).

35. J. Waguespack, F. T. Salles, B. Kachar, A. J. Ricci, Stepwise morphological and functional maturation of mechanotransduction in rat outer hair cells. *J. Neurosci. Off. J. Soc. Neurosci.* **27**, 13890–13902 (2007).

36. D. H. Sanes, S. Bao, Tuning up the developing auditory CNS. *Curr Opin Neurobiol* **19**, 188–199 (2009).

37. R. C. Froemke, B. J. Jones, Development of auditory cortical synaptic receptive fields. *Neurosci. Biobehav. Rev.* **35**, 2105–2113 (2011).

38. M. Nakamura, P. Valerio, S. Bhumika, T. R. Barkat, Sequential Organization of Critical Periods in the Mouse Auditory System. *Cell Rep.* **32**, 108070 (2020).

39. A. S. Keuroghlian, E. I. Knudsen, Adaptive auditory plasticity in developing and adult animals. *Prog. Neurobiol.* **82**, 109–121 (2007).

40. X. Zhou, M. M. Merzenich, Enduring effects of early structured noise exposure on temporal modulation in the primary auditory cortex. *Proc. Natl. Acad. Sci. U. S. A.* **105**, 4423–4428 (2008).

41. A. M. Lauer, B. J. May, B. R. J. M. Ay, A. M. Lauer, B. J. May, The medial olivocochlear system attenuates the developmental impact of early noise exposure. *JARO - J. Assoc. Res. Otolaryngol.* **12**, 329–343 (2011).

42. C. Caminos, E. Vale, R. Lujan, J. R. Martinez-Galan, J. M. Juiz, Developmental regulation and adult maintenance of potassium channel proteins (Kv 1.1 and Kv 1.2) in the cochlear nucleus of the rat. *Brain Res.* **1056** (2005).

43. A. L. Dorrn, K. Yuan, A. J. Barker, C. E. Schreiner, R. C. Froemke, Developmental sensory experience balances cortical excitation and inhibition. *Nature* **465**, 932–936 (2010).

44. Y. J. Sun, *et al.*, Fine-tuning of pre-balanced excitation and inhibition during auditory cortical development. *Nature* **465**, 927–931 (2010).

45. D. E. Vetter, *et al.*, Role of alpha9 nicotinic ACh receptor subunits in the development and function of cochlear efferent innervation. *Neuron* **23**, 93-103. (1999).

46. J. S. Buchwald, C. M. Huang, Far-field acoustic response: Origins in the cat. *Science* **189**, 382–384 (1975).

47. M. Karplus, C. Lee, W. J. Cashore, W. Oh, The effects of brain bilirubin deposition on auditory brain stem evoked responses in rats. *Early Hum. Dev.* **16**, 185–194 (1988).

48. S. M. Shapiro, Acute brainstem auditory evoked potential abnormalities in jaundiced Gunn rats given sulfonamide. *Pediatr. Res.* **23**, 306–310 (1988).

49. N. A. Shaw, The auditory evoked potential in the rat--a review. *Prog. Neurobiol.* **31**, 19–45 (1988).

50. J. Melcher, N. Y. Kiang, Generators of the brainstem auditory evoked potential in cat. III: Identified cell populations. *Hear. Res.* **93**, 52–71 (1996).

51. S. E. Kim, K. Turkington, C. Kushmerick, J. H. Kim, Central dysmyelination reduces the temporal fidelity of synaptic transmission and the reliability of postsynaptic firing during high-frequency stimulation. *J. Neurophysiol.* **110**, 1621–1630 (2013).

52. C. A. Shera, J. J. Guinan Jr., Evoked otoacoustic emissions arise by two fundamentally different mechanisms: a taxonomy for mammalian OAEs. *J Acoust Soc Am* **105**, 782–798 (1999).

53. L. Robles, M. A. Ruggero, Mechanics of the mammalian cochlea. *Physiol. Rev.* **81**, 1305–52 (2001).

54. D. Khimich, *et al.*, Hair cell synaptic ribbons are essential for synchronous auditory signalling. *Nature* **434**, 889–894 (2005).

55. A. Matsubara, J. H. Laake, S. Davanger, S. Usami, O. P. Ottersen, Organization of AMPA receptor subunits at a glutamate synapse: a quantitative immunogold analysis of hair cell synapses in the rat organ of Corti. *J. Neurosci.* **16**, 4457–4467 (1996).

56. L. D. Liberman, H. Wang, M. C. Liberman, Opposing gradients of ribbon size and AMPA receptor expression underlie sensitivity differences among cochlear-nerve/hair-cell synapses. *J. Neurosci. Off. J. Soc. Neurosci.* **31**, 801–8 (2011).

57. G. Sendin, J. Bourien, F. Rassendren, J.-L. Puel, R. Nouvian, Spatiotemporal pattern of action potential firing in developing inner hair cells of the mouse cochlea. *Proc. Natl. Acad. Sci. U. S. A.* **111**, 1999–2004 (2014).

58. M. Youssoufian, Development of a Robust Central Auditory Synapse in Congenital Deafness. *J. Neurophysiol.* **94**, 3168–3180 (2005).

59. R. N. Leao, *et al.*, Topographic organization in the auditory brainstem of juvenile mice is disrupted in congenital deafness. *J. Physiol.* **571**, 563–578 (2006).

60. J. J. Hirtz, *et al.*, Cav1.3 calcium channels are required for normal development of the auditory brainstem. *J. Neurosci. Off. J. Soc. Neurosci.* **31**, 8280–8294 (2011).

61. T. A. Babola, *et al.*, Purinergic Signaling Controls Spontaneous Activity in the Auditory System throughout Early Development. *J. Neurosci. Off. J. Soc. Neurosci.* **41**, 594–612 (2021).

62. T. Frank, D. Khimich, A. Neef, T. Moser, Mechanisms contributing to synaptic Ca2+ signals and their heterogeneity in hair cells. *Proc. Natl. Acad. Sci. U. S. A.* **106**, 4483–4488 (2009).

63. L. Sheets, K. S. Kindt, T. Nicolson, Presynaptic CaV1.3 channels regulate synaptic ribbon size and are required for synaptic maintenance in sensory hair cells. *J. Neurosci. Off. J. Soc. Neurosci.* **32**, 17273–17286 (2012).

64. H. C. Wong, *et al.*, Synaptic mitochondria regulate hair-cell synapse size and function. *eLife* **8**, e48914 (2019).

65. Ö. D. Özçete, T. Moser, A sensory cell diversifies its output by varying Ca2+ influx-release coupling among active zones. *EMBO J.* **40**, e106010 (2021).

66. S. Michanski, *et al.*, Mapping developmental maturation of inner hair cell ribbon synapses in the apical mouse cochlea. *Proc. Natl. Acad. Sci. U. S. A.* **116**, 6415–6424 (2019).

67. Y. Hua, *et al.*, Electron Microscopic Reconstruction of Neural Circuitry in the Cochlea. *Cell Rep.* **34**, 108551 (2021).

68. S. A. Payne, *et al.*, Maturation of Heterogeneity in Afferent Synapse Ultrastructure in the Mouse Cochlea. *Front. Synaptic Neurosci.* **13**, 678575 (2021).

69. H. M. Sobkowicz, J. E. Rose, G. E. Scott, S. M. Slapnick, Ribbon synapses in the developing intact and cultured organ of Corti in the mouse. *J Neurosci* **2**, 942–57. (1982).

70. A. Merchan-Perez, M. C. Liberman, Ultrastructural differences among afferent synapses on cochlear hair cells: correlations with spontaneous discharge rate. *J. Comp. Neurol.* **371**, 208–221 (1996).

71. L.-C. Huang, *et al.*, Synaptic profiles during neurite extension, refinement and retraction in the developing cochlea. *Neural Develop.* **7**, 38 (2012).

72. A. B. Wong, *et al.*, Developmental refinement of hair cell synapses tightens the coupling of Ca2+ influx to exocytosis. *EMBO J.* **33**, 247–264 (2014).

73. L. Song, J. McGee, E. J. Walsh, Frequency- and level-dependent changes in auditory brainstem responses (ABRS) in developing mice. *J. Acoust. Soc. Am.* **119**, 2242–2257 (2006).

74. K. A. Fernandez, P. W. C. Jeffers, K. Lall, M. C. Liberman, S. G. Kujawa, Aging after noise exposure : Acceleration of cochlear synaptopathy in “ recovered ” ears. *J. Neurosci.* **35**, 7509–20 (2015).

75. K. M. Schrode, M. L. Dent, A. M. Lauer, Sources of variability in auditory brainstem response thresholds in a mouse model of noise-induced hearing loss. *J. Acoust. Soc. Am.* **152**, 3576–3582 (2022).

76. Y. Lu, *et al.*, Spatial patterns of noise-induced inner hair cell ribbon loss in the mouse mid-cochlea. *iScience* **27**, 108825 (2024).

77. N. Rybalko, *et al.*, Development of the acoustic startle response in rats and its change after early acoustic trauma. *Behav. Brain Res.* **286**, 212–221 (2015).

78. L. Shi, *et al.*, Noise-induced damage to ribbon synapses without permanent threshold shifts in neonatal mice. *Neuroscience* **304**, 368–377 (2015).

79. N. I. Mohamad, *et al.*, Synaptic ribbon dynamics after noise exposure in the hearing cochlea. *Commun. Biol.* **7**, 421 (2024).

80. D. J. Moverman, L. D. Liberman, S. Kraemer, G. Corfas, M. C. Liberman, Ultrastructure of noise-induced cochlear synaptopathy. *Sci. Rep.* **13**, 19456 (2023).

81. S. Stamataki, H. W. Francis, M. Lehar, B. J. May, D. K. Ryugo, Synaptic alterations at inner hair cells precede spiral ganglion cell loss in aging C57BL/6J mice. *Hear. Res.* **221**, 104–118 (2006).

82. J. Y. Jeng, *et al.*, Pathophysiological changes in inner hair cell ribbon synapses in the ageing mammalian cochlea. *J. Physiol.* **598**, 4339–4355 (2020).

83. L. E. Boero, S. Payne, M. E. Gómez-Casati, M. A. Rutherford, J. D. Goutman, Noise Exposure Potentiates Exocytosis From Cochlear Inner Hair Cells. *Front. Synaptic Neurosci.* **13**, 740368 (2021).

84. K. Suthakar, M. C. Liberman, Auditory-Nerve Responses in Mice with Noise-Induced Cochlear Synaptopathy. *https://doi.org/10.1152/jn.00342.2021* (2021). https://doi.org/10.1152/JN.00342.2021.

85. M. B. Wood, *et al.*, Acoustic Trauma Increases Ribbon Number and Size in Outer Hair Cells of the Mouse Cochlea. *J. Assoc. Res. Otolaryngol. JARO* **22**, 19–31 (2021).

86. A. C. Furman, S. G. Kujawa, M. C. Liberman, Noise-induced cochlear neuropathy is selective for fibers with low spontaneous rates. *J. Neurophysiol.* **110**, 577–586 (2013).

87. J. Schindelin, *et al.*, Fiji: an open-source platform for biological-image analysis. *Nat. Methods* **9**, 676–82 (2012).

88. D. Sage, *et al.*, DeconvolutionLab2: An open-source software for deconvolution microscopy. *Methods* **115**, 28–41 (2017).

89. Z. Jing, *et al.*, Disruption of the presynaptic cytomatrix protein bassoon degrades ribbon anchorage, multiquantal release, and sound encoding at the hair cell afferent synapse. *J. Neurosci.* **33**, 4456–4467 (2013).

90. F. Gilels, S. T. Paquette, J. Zhang, I. Rahman, P. M. White, Mutation of foxo3 causes adult onset auditory neuropathy and alters cochlear synapse architecture in mice. *J. Neurosci.* **33**, 18409–18424 (2013).

91. S. T. Paquette, F. Gilels, P. M. White, Noise exposure modulates cochlear inner hair cell ribbon volumes, correlating with changes in auditory measures in the FVB/nJ mouse. *Sci. Rep.* **6**, 1–13 (2016).

92. J. Ollion, J. Cochennec, F. Loll, C. Escudé, T. Boudier, TANGO: A generic tool for high-throughput 3D image analysis for studying nuclear organization. *Bioinformatics* **29**, 1840–1841 (2013).

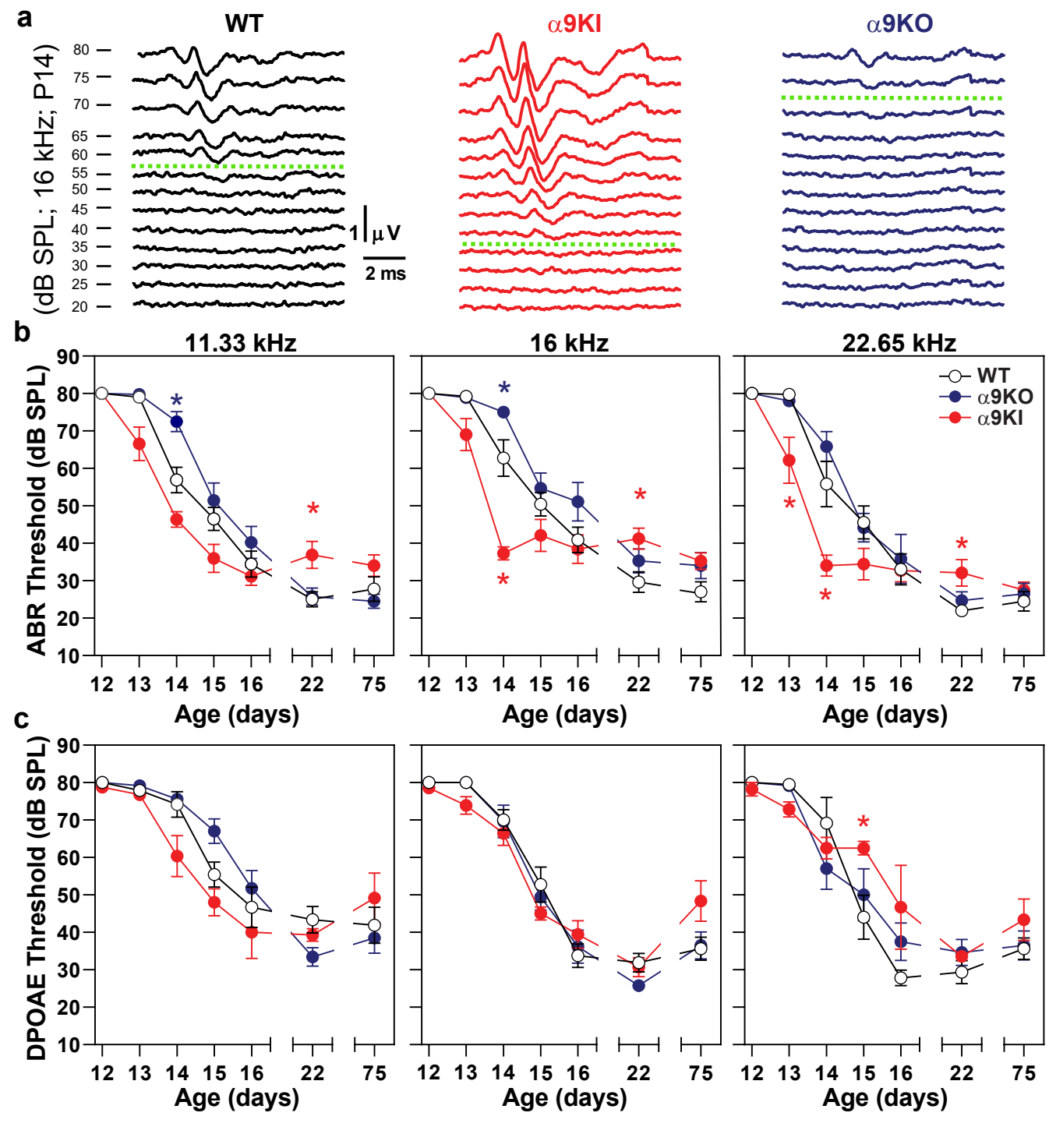
a
WT
α9KI
α9KO
(dB SPL; 16 kHz; P14)
80
75
70
65
60
55
50
45
40
35
30
25
20
1 μV
2 ms
b
11.33 kHz
16 kHz
22.65 kHz
ABR Threshold (dB SPL)
WT
α9KO
α9KI
Age (days)
c
DPOAE Threshold (dB SPL)
Age (days)

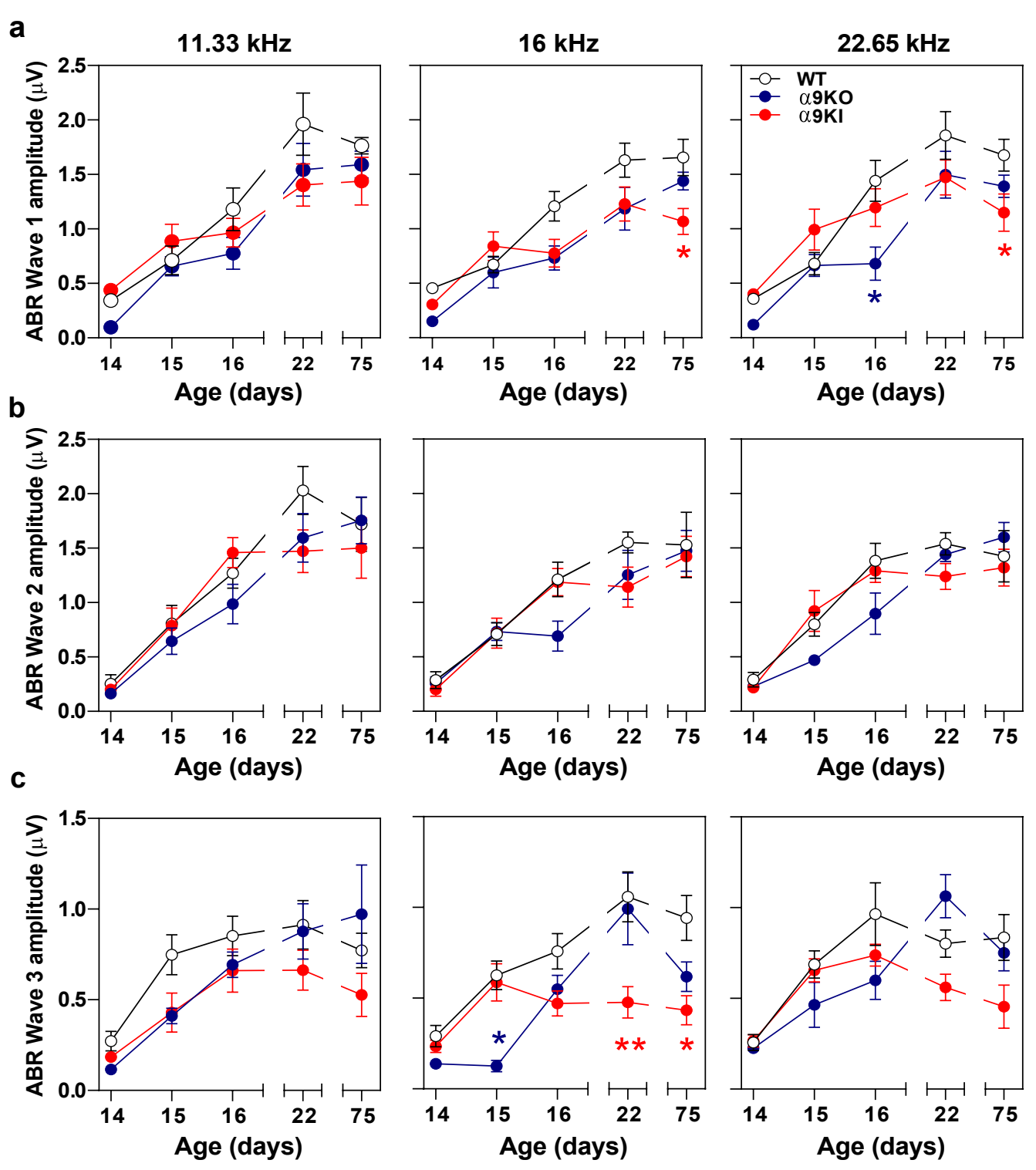
a
11.33 kHz
16 kHz
22.65 kHz
WT
α9KO
α9KI
ABR Wave 1 amplitude (μV)
2.5
2.0
1.5
1.0
0.5
0.0
14
15
16
22
75
Age (days)
*
*
*
b
ABR Wave 2 amplitude (μV)
2.5
2.0
1.5
1.0
0.5
0.0
14
15
16
22
75
Age (days)
c
ABR Wave 3 amplitude (μV)
1.5
1.0
0.5
0.0
14
15
16
22
75
Age (days)
*
**
*

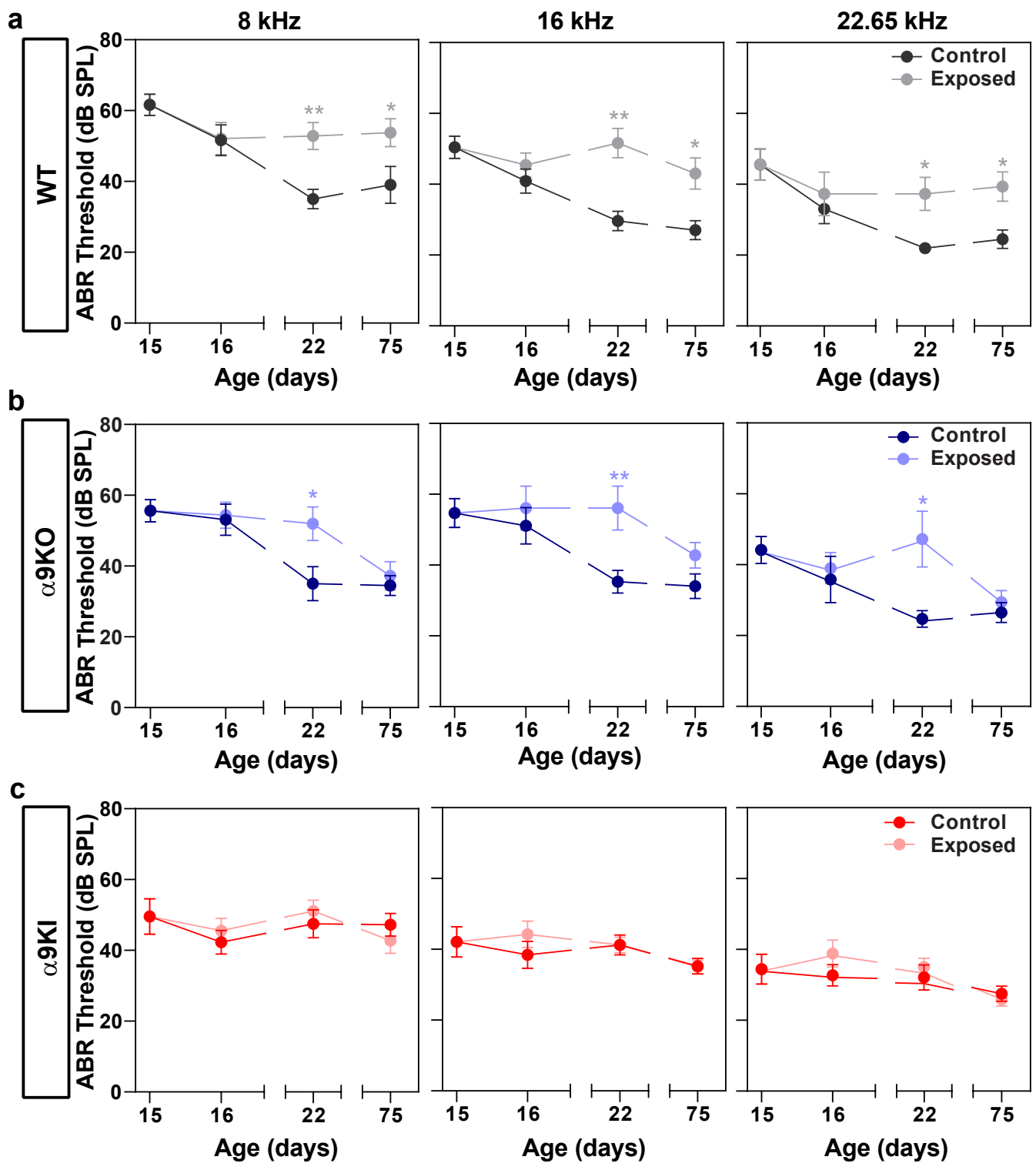
a
8 kHz
16 kHz
22.65 kHz
WT
ABR Threshold (dB SPL)
Control
Exposed
Age (days)
b
α9KO
c
α9KI

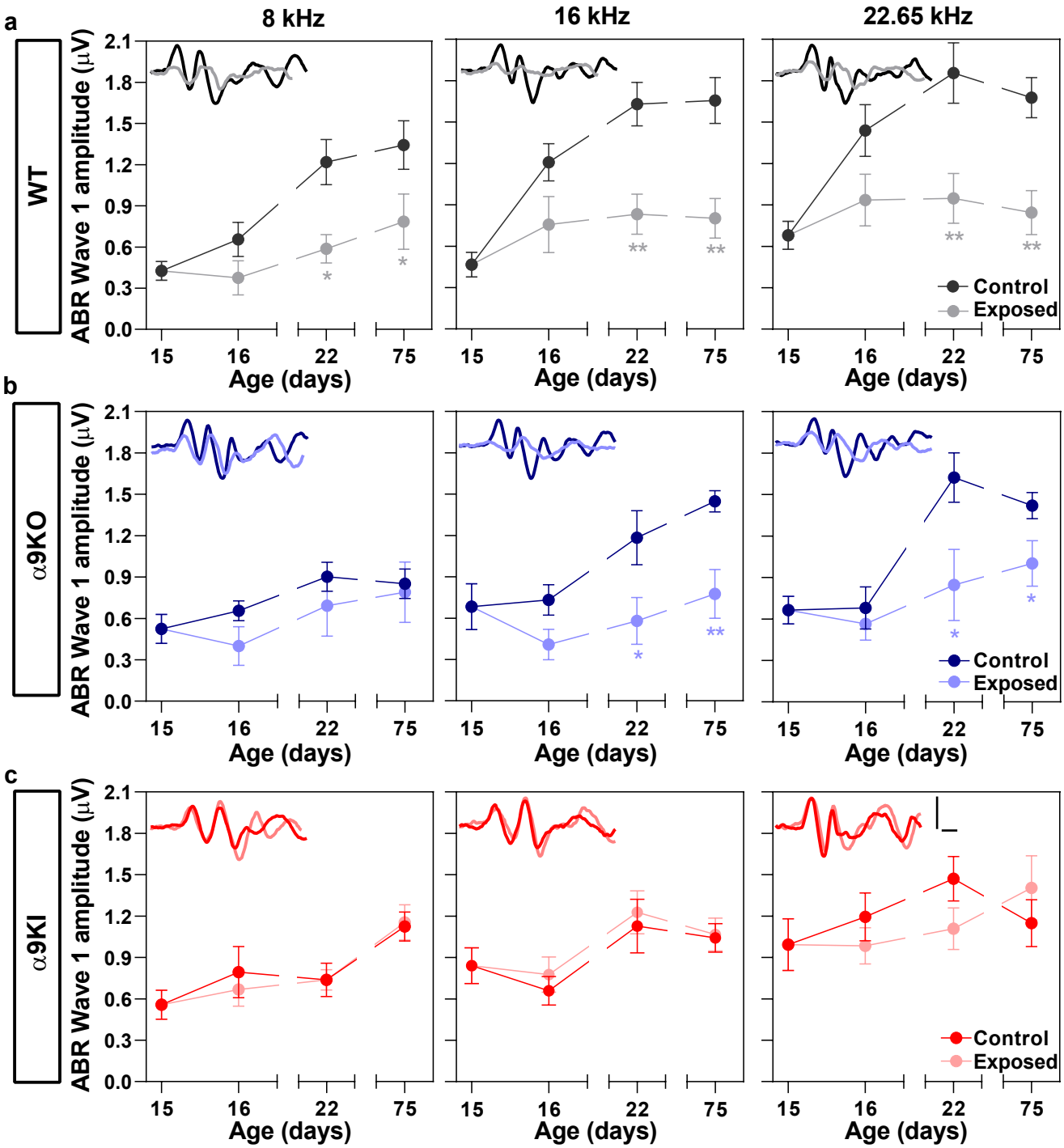
a
8 kHz
16 kHz
22.65 kHz
WT
ABR Wave 1 amplitude (μV)
2.1
1.8
1.5
1.2
0.9
0.6
0.3
0.0
15
16
22
75
Age (days)
*
**
Control
Exposed
b
α9KO
c
α9KI

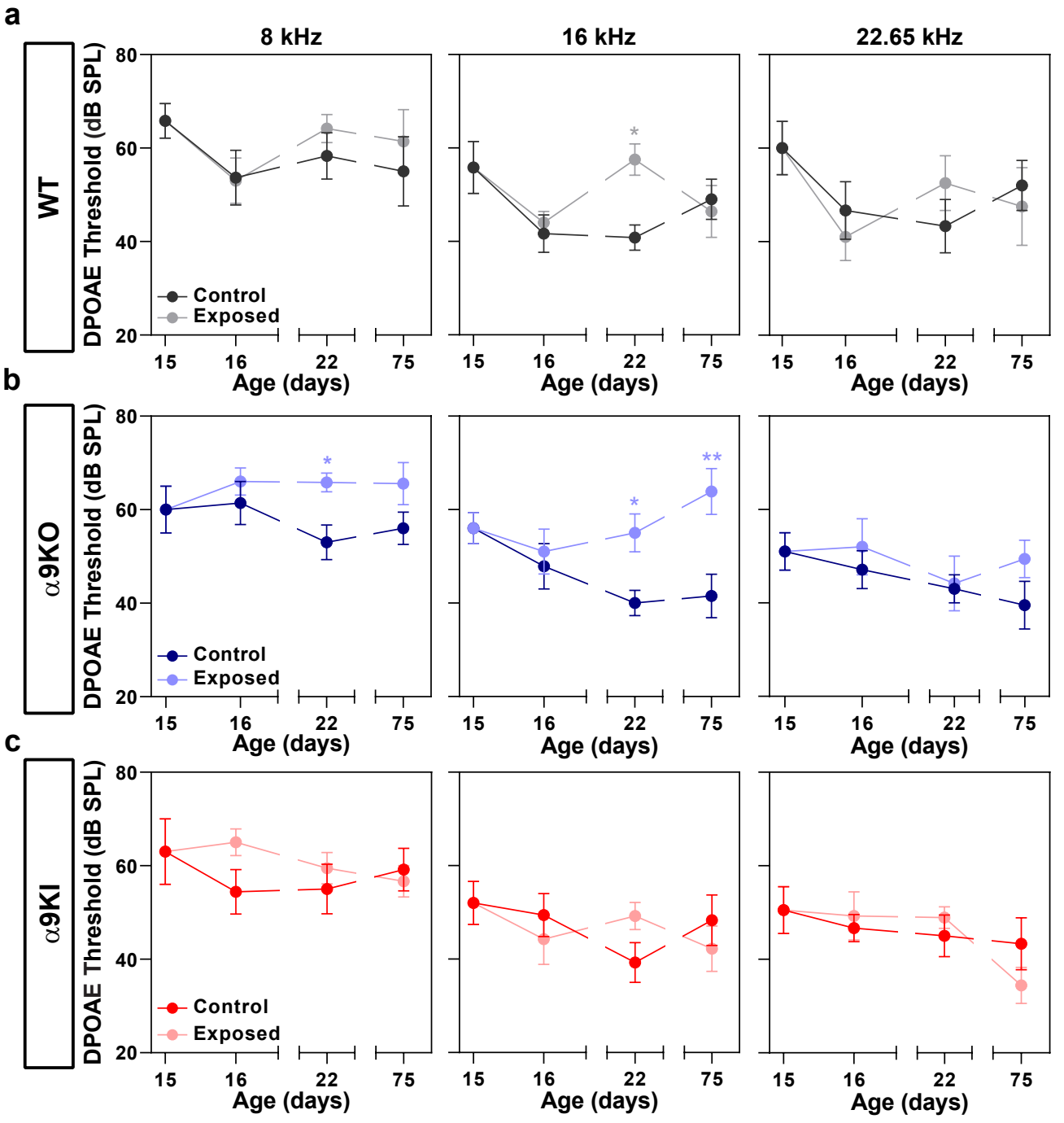
a
8 kHz
16 kHz
22.65 kHz
WT
DPOAE Threshold (dB SPL)
80
60
40
20
Control
Exposed
*
15
16
22
75
Age (days)
b
α9KO
*
*
**
c
α9KI

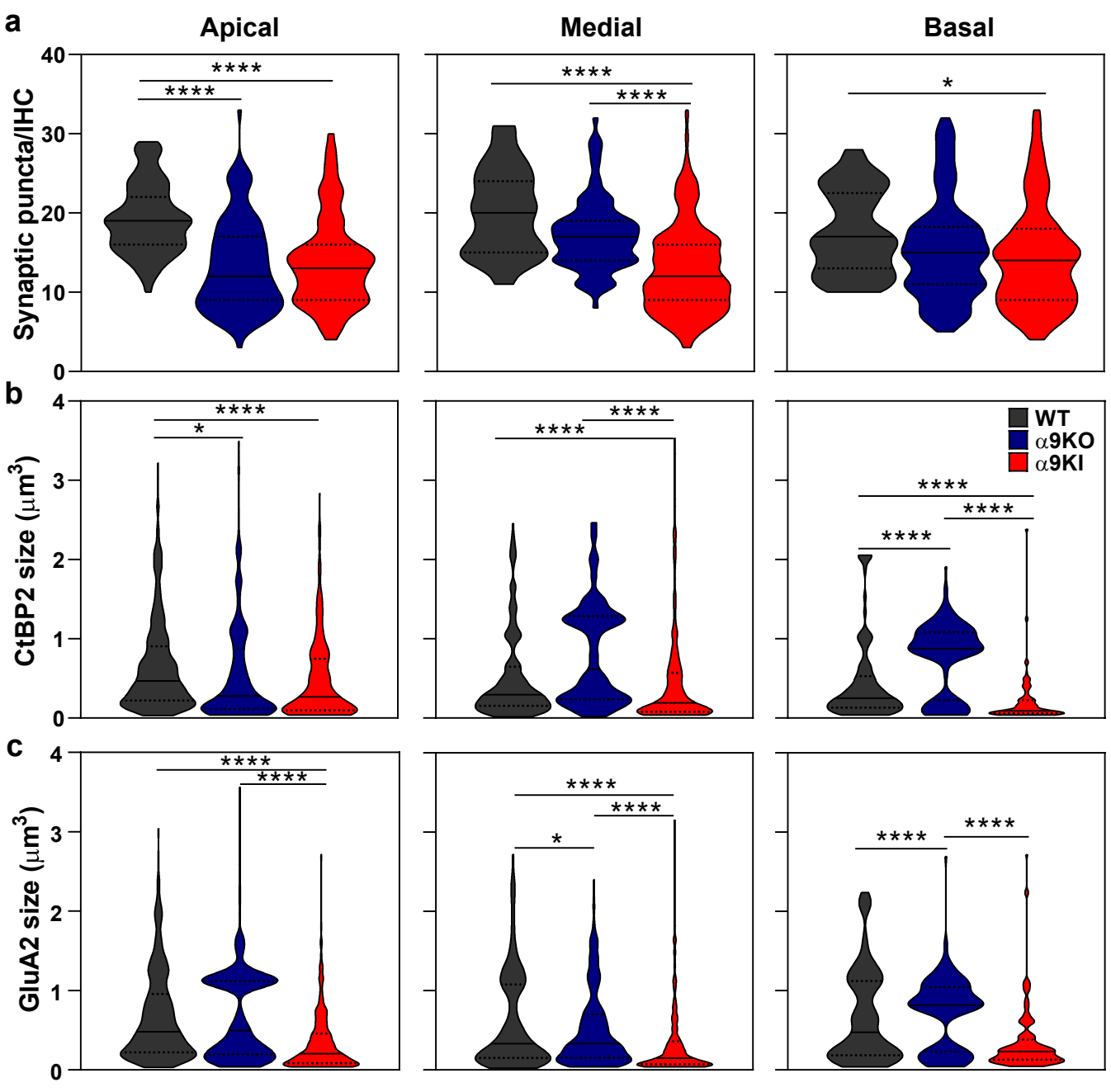
a
Apical
Medial
Basal
Synaptic puncta/IHC
40
30
20
10
0
****
****
****
****
*
b
CtBP2 size (μm3)
4
3
2
1
0
****
*
****
****
****
****
****
****
****
WT
α9KO
α9KI
c
GluA2 size (μm3)
4
3
2
1
0
****
****
****
****
*
****
****
****

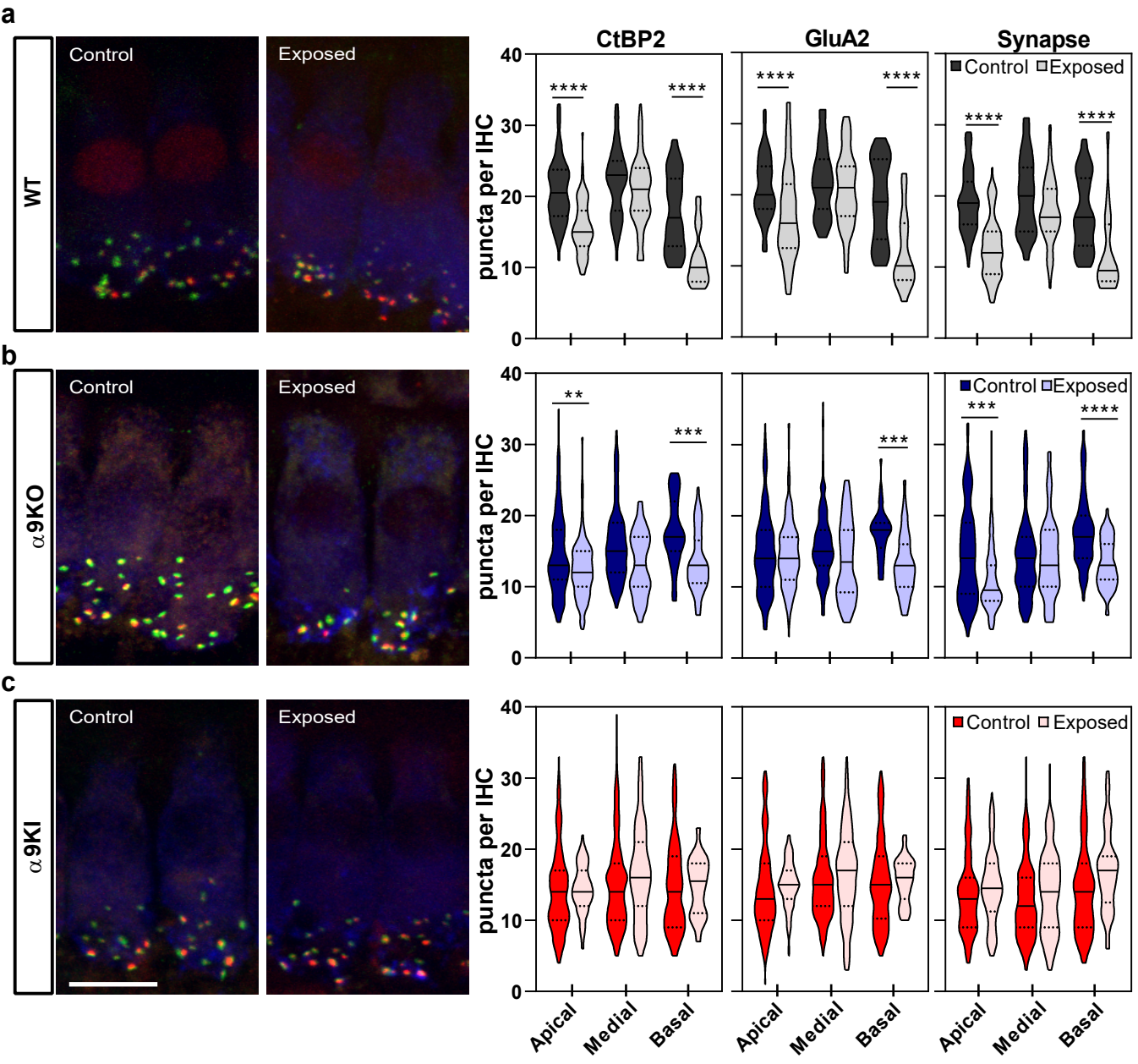
a
WT
Control
Exposed
CtBP2
GluA2
Synapse
Control
Exposed
puncta per IHC
****
b
α9KO
**
***
c
α9KI
Apical
Medial
Basal

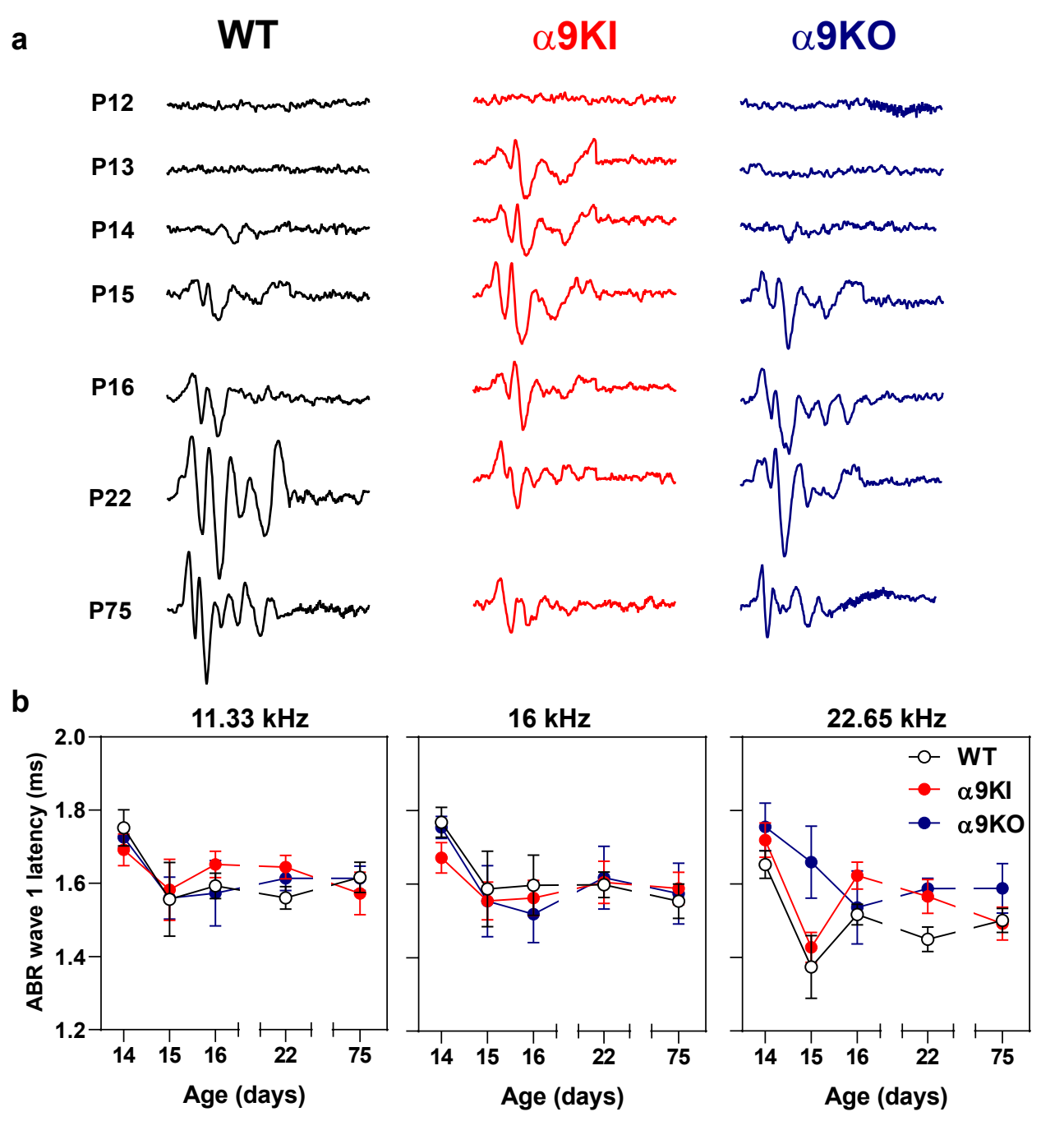
a
WT
α9KI
α9KO
P12
P13
P14
P15
P16
P22
P75
b
11.33 kHz
16 kHz
22.65 kHz
ABR wave 1 latency (ms)
2.0
1.8
1.6
1.4
1.2
14
15
16
22
75
Age (days)
WT
α9KI
α9KO